Received: 27 June 2023 | Revised: 9 September 2023 | Accepted: 15 September 2023

DOI: 10.1002/esp.5713

RESEARCH ARTICLE

ESPL WILEY

Periglacial resurfacing of hillslopes and channels with large boulders in the Virginia Appalachians

Michelle L. Fame[1,2] | Kristin D. Chilton[3,4] | James A. Spotila[5] | Meredith A. Kelly[2] | Summer A. Caton[6]

[1]Department of Geology, Amherst College, Amherst, Massachusetts, USA

[2]Department of Earth Sciences, Dartmouth College, Hanover, New Hampshire, USA

[3]Department of Geology and Geography, West Virginia University, Morgantown, West Virginia, USA

[4]Department of Civil and Environmental Engineering, Virginia Tech, Blacksburg, Virginia, USA

[5]Department of Geosciences, Virginia Tech, Blacksburg, Virginia, USA

[6]Department Earth and Space Sciences, University of Washington, Seattle, Washington, USA

Correspondence
Michelle L. Fame, Department of Geology, Amherst College, Beneski Earth Sciences Building, Amherst, MA 01002, USA.
Email: mfame@amherst.edu

Funding information
Purdue Rare Isotope Measurement Laboratory (PRIME) Seed Analyses Award; Dartmouth College Earth Sciences Obering Postdoctoral Fellowship

Abstract

Large, resistant, quartz-rich boulders deposited on hillslopes and in channels armour the landscape, trap sediment and influence hillslope angle and erodibility. In the Virginia Appalachians, such boulders are a significant component of hillslopes and channels. Establishing the timing of and processes responsible for bedrock fracture and boulder deposition is a critical piece of understanding the landscape as a system. In this study, we use cosmogenic ^{10}Be exposure dating to resolve the timing of boulder deposition at three sites in the Virginia Valley and Ridge province: Gap Mountain, Brush Mountain and Little Stony Creek, and at one site in the Virginia Blue Ridge: Devil's Marbleyard. The correlation between measured boulder exposure ages (101.7 ± 6.9 ka to 10.8 ± 0.8 ka; $n = 23$) and the Wisconsin Glacial Stage and subsequent Laurentide Ice Sheet (LIS) deglaciation (~115–11.7 ka) suggests a periglacial origin for deposition of large hillslope and channel boulders in the Virginia Appalachians. The lack of boulder exposure ages corresponding to the Last Interglacial Stage or following Wisconsin LIS retreat suggests interglacial non-deposition and stability. The absence of exposure ages from the penultimate Illinoian or older Quaternary Glacial Stages suggests that periglacial hillslope processes allow the landscape to be resurfaced with large boulders during each return to cold climate conditions. This cyclic resurfacing of hillslopes and channels is an example of how climatic oscillations insert disequilibrium into the landscape cycle and contributes to our appreciation of the timescales over which contemporary climate change may impact boulder dominated landscapes in rapidly warming alpine and arctic environments.

KEYWORDS
boulder deposits, periglacial geomorphology, quaternary geochronology

1 | INTRODUCTION

Large boulders deposited on hillslopes and in channels exert a significant geomorphic influence on the landscape. On hillslopes, boulders sourced from resistant ridge-forming lithologies may armour less resistant underlying rocks (Glade et al., 2017) and trap sediment (Glade & Anderson, 2018), leading to a decrease in erosion rates allowing steep slopes to persist longer than uncovered counterparts (Granger et al., 2001). In headwater channels, large boulders that are not moved by water flow act to impede erosion and steepen channels (Shobe et al., 2016, 2018; Sklar & Dietrich, 2001). Larger fracture spacing within ridge-forming bedrock generally leads to larger and less mobile boulders on hillslopes and in channels, impeding erosion, and resulting in catchments with higher relief and steeper channels than their counterparts with closer fracture spacing (DiBiase et al., 2018; Thaler & Covington, 2016). Constraining the depositional timing and residence time of large boulders on hillslopes and in channels contributes to our understanding of the processes responsible for their generation and is important to our understanding of erosion and topographic changes across the landscape system.

In the southern Appalachians (Figures 1 and 2), large boulders are a major component of hillslopes and headwater channels (Mills, 1981; Nelson et al., 2007). In the Paleozoic fold and thrust belt of the Virginia Valley and Ridge province, boulders sourced from quartz rich siliciclastic ridgeline lithologies have been quantified as covering up to 9% of hillslope area, 20–90% of headwater channel area, and are inferred to armour the underlying less resistant units, such as shales and limestones (Chilton & Spotila, 2020) (Figures 3 and 4). In the metamorphic rocks of the Virginia Blue Ridge province, unvegetated Cambrian quartzite boulder fields are common features, starkly visible along the western flank of the otherwise heavily forested area just east of the Blue Ridge Fault (Figures 5 and S1).

In this study, we use terrestrial cosmogenic nuclide ^{10}Be surface exposure dating to resolve the timing of boulder deposition at three sites in the Virginia Valley and Ridge province and at one site in the Blue Ridge (Figure 2). Devil's Marbleyard is a well-known boulder field and iconic landscape feature in the Virginia Blue Ridge and previous work from the Valley and Ridge sites has highlighted the prevalence and geomorphic importance of large boulders on hillslopes and in channels in the southern Appalachians (Chilton & Spotila, 2020; Mills, 1981, 1990). In these and other similar landscapes it has long been speculated that the production of their characteristic boulder deposits resulted from ice sheet proximal or 'periglacial' frost cracking of ridgeline bedrock during Quaternary Glacial Stages leading to the release and deposition of large boulders on hillslopes and in channels (e.g., Chilton & Spotila, 2020; Merritts & Rahnis, 2022; Mills, 1981; Nelson et al., 2007). However, their origins have yet to be directly tied to a specific time or process.

This work contributes to the complexity driven disequilibrium model for the topographic evolution of the Appalachian Mountains (Spotila & Prince, 2022). This model suggests that the geomorphic response to climatic changes might mimic the erosional or topographic

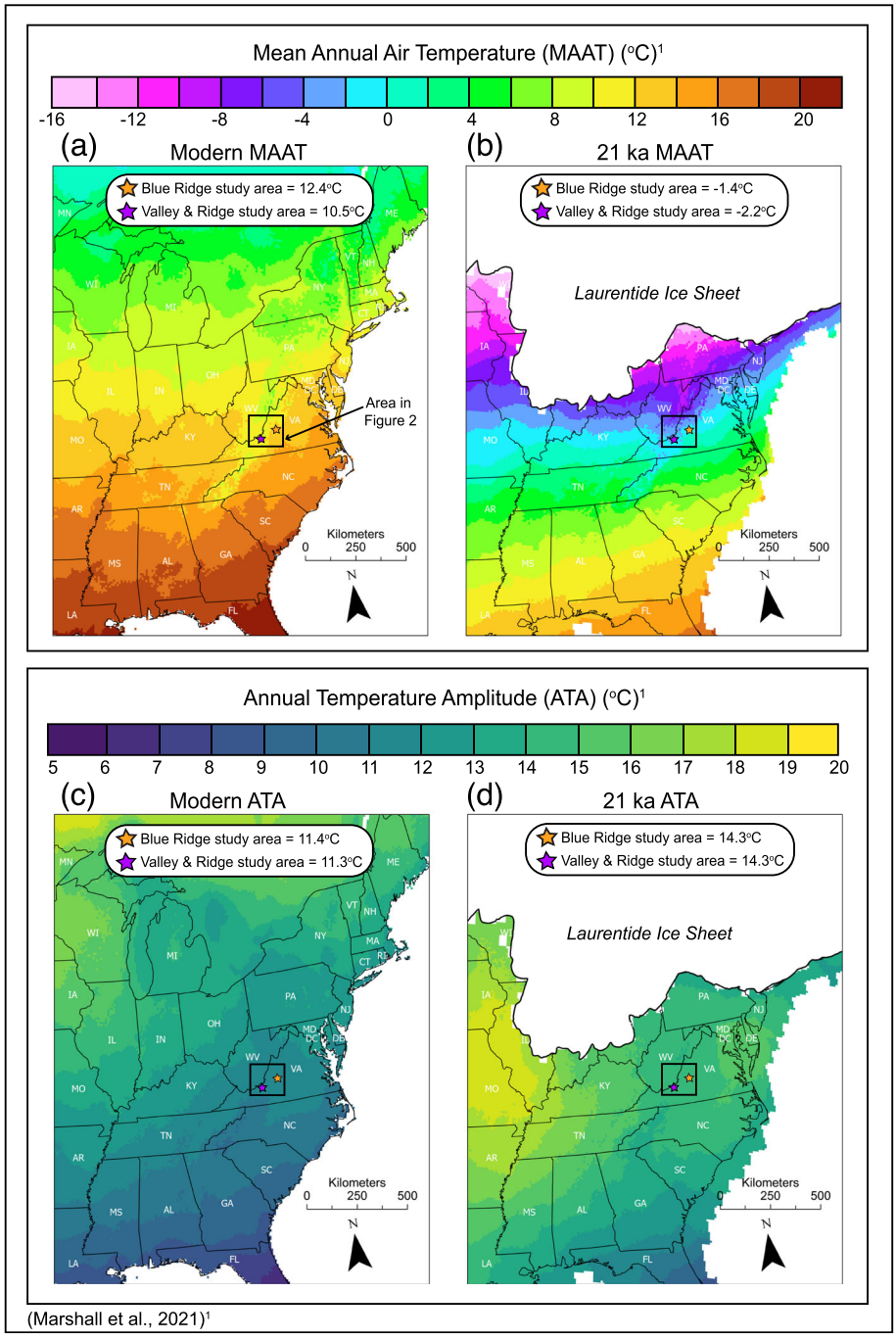

FIGURE 1 The (a) modern and (b) 21 ka LGM mean annual air temperature (MAAT) and (c) modern and (d) mean annual temperature amplitude (ATA) datasets displayed in these four maps are derived from the ensemble climate models presented in Marshall et al. (2021). The data used to make these maps are described in and are available for download in the supplementary material associated with the Marshall et al. (2021) publication. In each map, the orange star indicates the location of the Blue Ridge study area, the purple star indicates the location of the Valley and Ridge study area and the black inset box demarcates the map area presented in Figure 2.

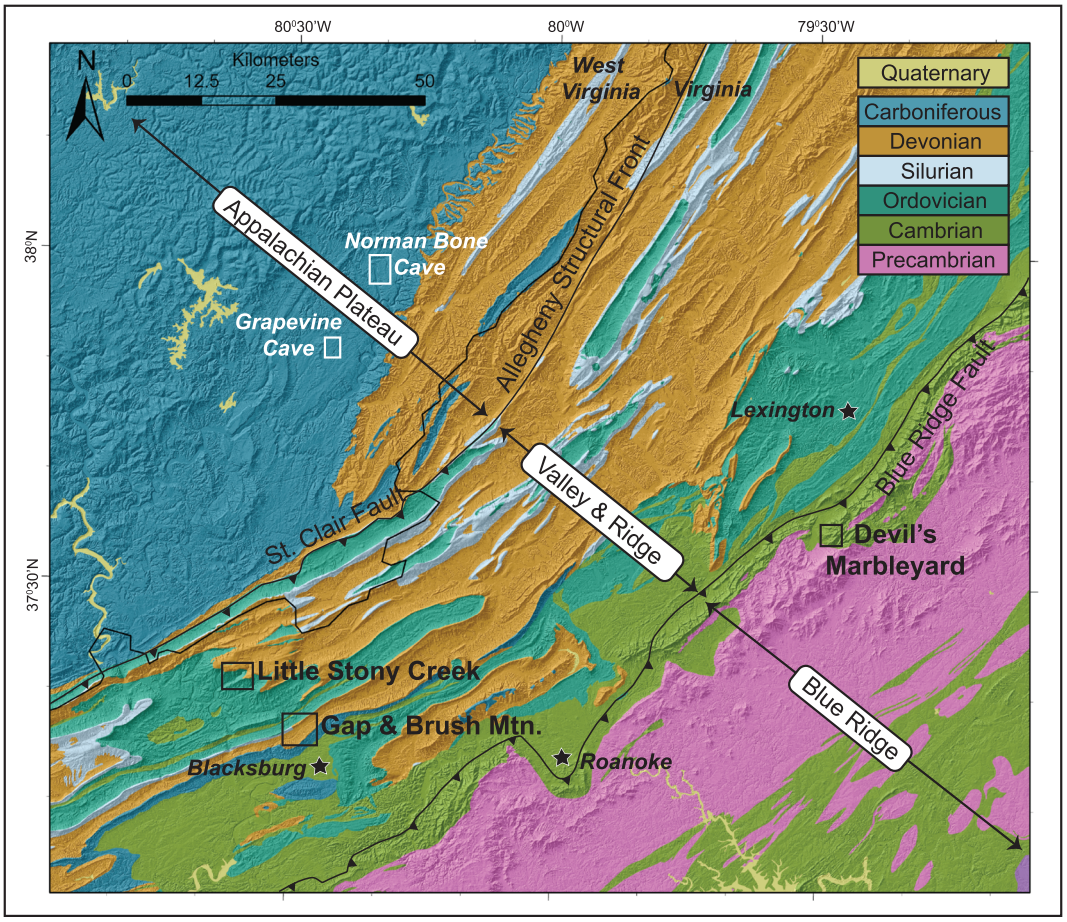

FIGURE 2 This map of the West Virginia and Virginia border region (area from the inset box shown in Figure 1) displays topography, simplified bedrock geology, regional geologic provinces, and the location of study sites. Bedrock geology is derived from the United States Geological Survey State Geologic Map Compilation (USGS SGMC) database (Horton, 2017) and is colour coded based upon geologic age (see key in map). Samples collected for this study from the Virginia Valley and Ridge province were taken from Gap Mountain, Brush Mountain and Little Stony Creek. Samples collected for this study from the Blue Ridge were taken from Devil's Marbleyard. Also shown on this map are the locations of Norman Bone Cave and Grapevine Cave in the West Virginia Appalachian Plateau; these caves are the site of the speleothem climate proxies of Thompson et al. (1976) that are displayed in Figure 6d.

signals commonly assigned to other forces such as mantle dynamics, tectonic uplift, intrinsic lithologic differences or erosional isostatic adjustment and vice versa. By investigating the extent to which boulder deposits in the southern Appalachians are or are not tied to periglacial conditions, we also contribute to a developing appreciation of the timescales over which we might anticipate major changes in Arctic and alpine hillslope stability and sediment supply resulting from contemporary global warming (Delunel et al., 2010; Haeberli et al., 2004; Hales & Roering, 2005; Krautblatter et al., 2012; Peizhen et al., 2001; Rowland et al., 2010; Sklar et al., 2017).

2 | LITERATURE REVIEW

2.1 | Geologic and geomorphic setting

Our study areas span two geologic provinces in the central Appalachian Mountains—the Virginia Valley and Ridge province, a Paleozoic foreland basin fold and thrust belt, and the Virginia Blue Ridge, a Cambrian and Precambrian basement thrust sheet (Figure 2). In the Valley and Ridge, we measured ^{10}Be exposure ages ($n = 12$) of large boulders on hillslopes and in channels from three study sites at elevations ranging from 694 to 811 m above mean sea level (amsl) and located ~15–25 km west of Blacksburg, Virginia: Gap Mountain, Brush Mountain and Little Stony Creek (Figures 3 and 4). In the Blue Ridge, we measured ^{10}Be exposure ages of boulders ($n = 11$) spanning an elevation range of 538 to 705 m amsl along the length Devil's Marbleyard, a southwest-facing boulder field located ~20 km south of Lexington, Virginia (Figure 5).

Boulder-producing units at Gap Mountain and Little Stony Creek are the Silurian Tuscarora Sandstone and the Devonian Keefer Sandstone (Figures 3 and 4). The Tuscarora Sandstone has a stratigraphic thickness of between 15 and 45 m and is composed of well-sorted fine to medium sand framework grains that are 98% quartz. It has <1% porosity, is recrystallized and has one of the highest erosivity resistance indices in the Valley and Ridge (Chilton & Spotila, 2020; Hale & Shakoor, 2003). The Keefer Sandstone has a stratigraphic thickness of 65–70 m and is composed of fine sand framework grains that are 97% quartz cemented with silica and haematite cement (Bartholomew et al., 2000; Mills, 1990, 2003; Raymond et al., 2014). The boulder-producing unit on Brush Mountain is the Cloyd Conglomerate, the basal member of the Mississippian Price Formation (Figure 3). The Cloyd Conglomerate is a well-cemented quartz pebble conglomerate composed of grains ranging from 0.1 mm to 2 cm, 98%

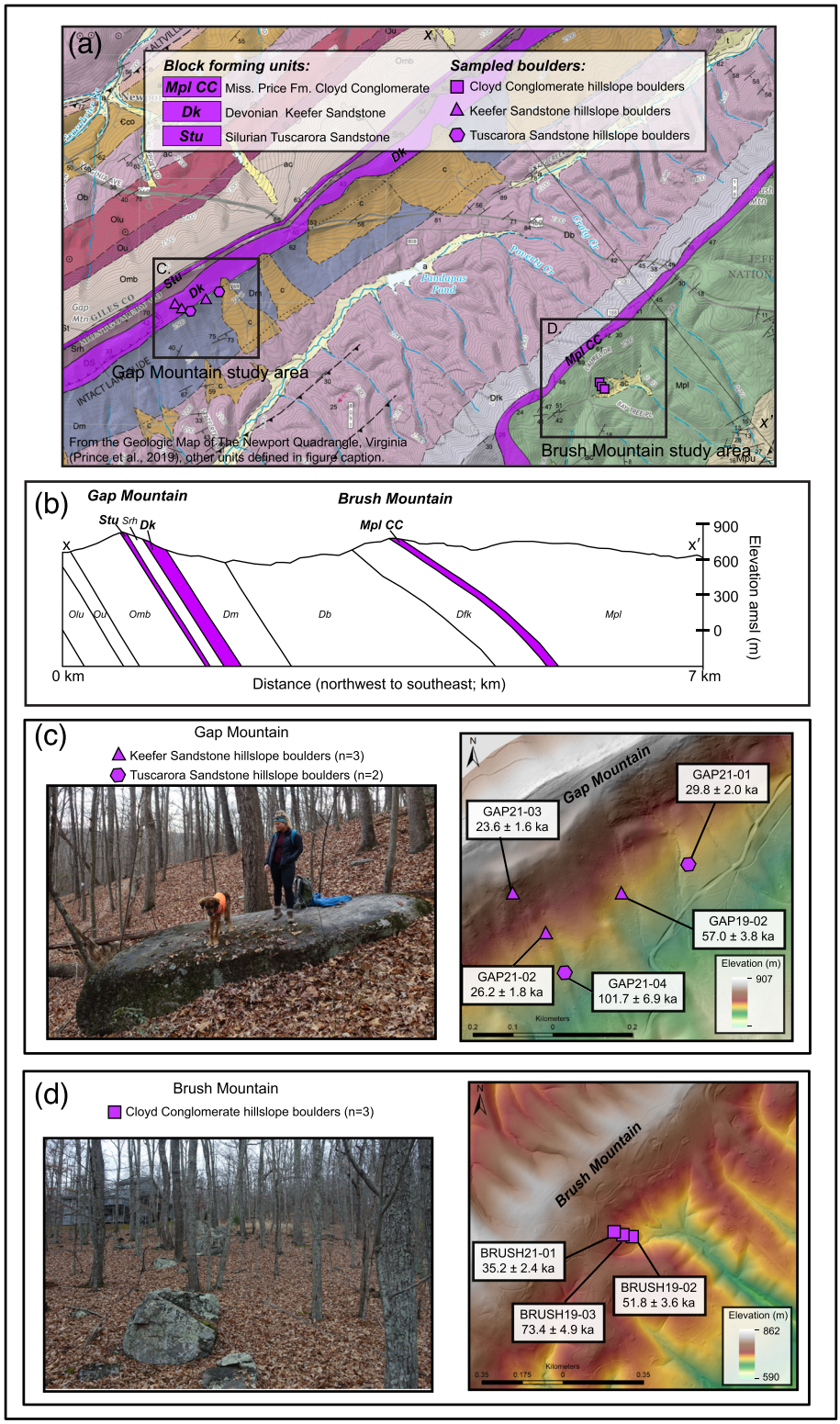

FIGURE 3 (a) The geologic setting for the Gap Mountain and Brush Mountain study areas from the Geologic Map of the Newport Quadrangle, Virginia (Prince et al., 2019), includes the following major bedrock units: Ordovician—Martinsburg Formation (Omb; grey shale, siltstone, wacke and limestone); Silurian—Tuscarora Formation (Stu; medium to coarse grained orthoquartzite with occasional conglomerate lenses) and Rose Hill Formation (Srh—maroon fine-grained sandstone with shale interbeds); Devonian—Keefer sandstone (Dk; light grey sandstone with minor siltstone), Millboro Formation (Dm; shale with minor sandstone and limestone interbeds), Brailler Formation (Db; interbedded shale and fine sandstone) and Foreknobs Fm. (Dfk—sandstone with siltstone, red shale and fossil hash); Mississippian—Price Formation Cloyd Conglomerate member (Mpl CC; basal quartz pebble conglomerate and white sandstone) of the Price Formation (Mpl; sandstone and shale). Boulder forming units (highlighted in purple) in the Gap Mountain study are the Tuscarora Formation (Stu) the Keefer Formation (Dk) and in the Brush Mountain study area is the Cloyd Conglomerate member of the Price Formation. Sampled boulders from those units are shown (respectively) as purple hexagon, triangle and square markers. (b) Geology is shown in cross section from x-x′ with approximate boulder sample sites included at the surface by their respective markers. (c) The Gap Mountain study area with an example sample site photograph, lidar hill shade map and cosmogenic exposure ages. Inset location shown above. (d) The Brush Mountain study area with an example sample site photograph, lidar hill shade map and cosmogenic exposure ages. Inset location shown above in (a). For annotated photographs of all sampled boulders, see Figure S2.

of which are quartz. It has <2% porosity, a total stratigraphic thickness of 12–20 m, and is considered a ridge-forming unit though it does not always outcrop along ridges because it is buried beneath modern soils (Bartholomew et al., 2000). Shale, mudstones, siltstones and limestones sometimes interbedded with thin sandstone layers comprise the lower elevation units on which large boulders occur (Prince et al., 2019; Schultz et al., 1986), suggesting that hillslope armouring is a likely result of these boulder accumulations (Chilton & Spotila, 2020) (Figures 3 and 4). Mean and maximum slope angles (respectively) are 12° and 37° at Gap Mountain, 12° and 33° at Brush Mountain and 18° and 40° on the hillslopes surrounding Little Stony Creek.

Devil's Marbleyard boulder field is ~100 m wide and ~380 m long, has a mean slope angle of 28°, and has nearly 100% boulder cover, excluding the fractured outcrops at the top and middle of the boulder field (Figure 5). Directly below the boulder field, the James River headwater stream Belfast Creek drains the valley. Boulder lithology is Cambrian Chilhowie Group Antietam Quartzite, a well-cemented and recrystallized quartz arenite containing skolithos

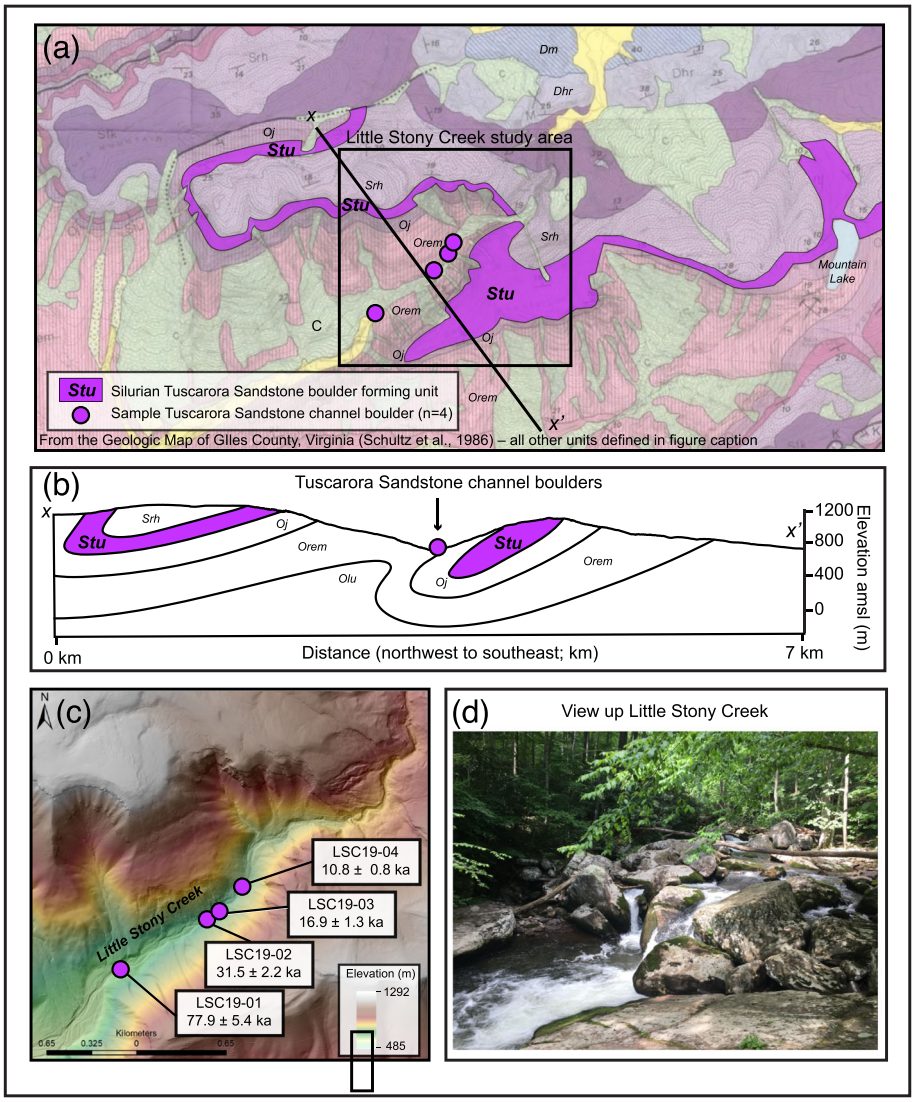

FIGURE 4 (a) The geologic setting for the Little Stony Creek study area is from the Geologic Map of Giles County, Virginia (Schultz et al., 1986), and includes the following major bedrock units: Ordovician—undivided limestones (Olu), Reedsville, Eggleston and Moccasin Formations (Orem; limestones, mudstones and siltstones) and Juniata Formation (Oj; sandstone, siltstone and shale); Silurian—Huntersville and Rocky Gap Formations (Dhr; chert and calcareous sandstone), Tuscarora Formation (Stu; medium to coarse grained orthoquartzite with occasional conglomerate lenses), Rose Hill Formation (Srh—maroon fine grained sandstone with shale interbeds) and Tonoloway limestone and Keefer sandstone (Stk); Devonian—Millboro Shale (Dm). The major boulder forming unit (highlighted in purple) in the Little Stony Creek study is Tuscarora Formation (Stu). Sampled Tuscarora channel boulder is marked by purple circles. (b) Geology is shown in cross section from x-x′ with approximate boulder sample location in cross section shown at the surface. (c) The Little Stony Creek study area is shown with a lidar hillshade map and cosmogenic exposure ages. Inset location shown in (a). (d) Photograph shows the view up the little Stony Creek study area highlighting the prevalence of large channel boulders. For annotated photographs of all sampled boulders, see Figure S2.

burrow trace fossils with total unit thickness ranging from 120 to 365 m (Brown & Spencer, 1981; Fichter et al., 2010; Schwab, 1970) (Figure 5). During the Alleghenian Orogeny in the late Paleozoic Era, the Blue Ridge thrust fault system (Figure 2) emplaced hanging wall Blue Ridge basement rocks over the footwall Paleozoic strata of the Valley and Ridge Province. Movement along the Blue Ridge fault imprinted a brittle deformation fabric on adjacent rocks, and it is characterized by extensive jointing due to deformation during both Alleghenian thrusting and subsequent Mesozoic extension (Fichter et al., 2010).

In both the Valley and Ridge and Blue Ridge study sites, boulder source is clear because of lithology, but the mechanisms of boulder detachment, transport, deposition and likelihood of post-depositional stability is different and not clear in all cases. In Little Stony Creek, sampled boulders have long axes between 5 and 11 m, occur in the creek bed, and are sourced from a cliff of Tuscarora Sandstone located high above the stream valley (Table 1 and Figures 4 and S2). These boulders were presumably transported as rockfall upon detachment and deposited on the valley floor. As a result of their size and current low potential energy position on the valley floor, they are likely to have been stable since deposition. 2003Tuscarora Sandstone boulders also occur on the hillslopes adjacent to Little Stony Creek (Mills, 1990), but access conditions during fieldwork did not allow us to sample them. At Gap and Brush Mountains, sampled boulders were tabular and blocky with long axes between 3 and 7 m and are aligned subparallel to the steepest slope angle (Table 1 and Figures 3 and S2). Upon detachment from ridgeline source units, these boulders likely fell and rolled on the hillslope surface before being deposited in their modern orientations. It is possible that these boulders have been moved or modified by hillslope processes following initial deposition, via mechanism such as creep processes, stochastic storm events, or they may even have been core pieces of larger debris flows that have since eroded away. At Devil's Marbleyard, the origin of sampled boulders, with long axes between 2 and 5 m, is the still-present outcrops of fractured bedrock at the uphill edge and midpoint of the boulder field (Table 1 and Figures 5 and S2). The mechanisms responsible for triggering the formation of Devil's Marbleyard and whether it formed instantaneously as a stochastic rockfall or over a prolonged period as a slow topple-style failure remain unclear.

2.2 | Frost cracking and prior evidence of regional periglacial processes

Frost cracking dominantly results from the accumulation of stresses generated by subcritical cracking during segregation ice because the

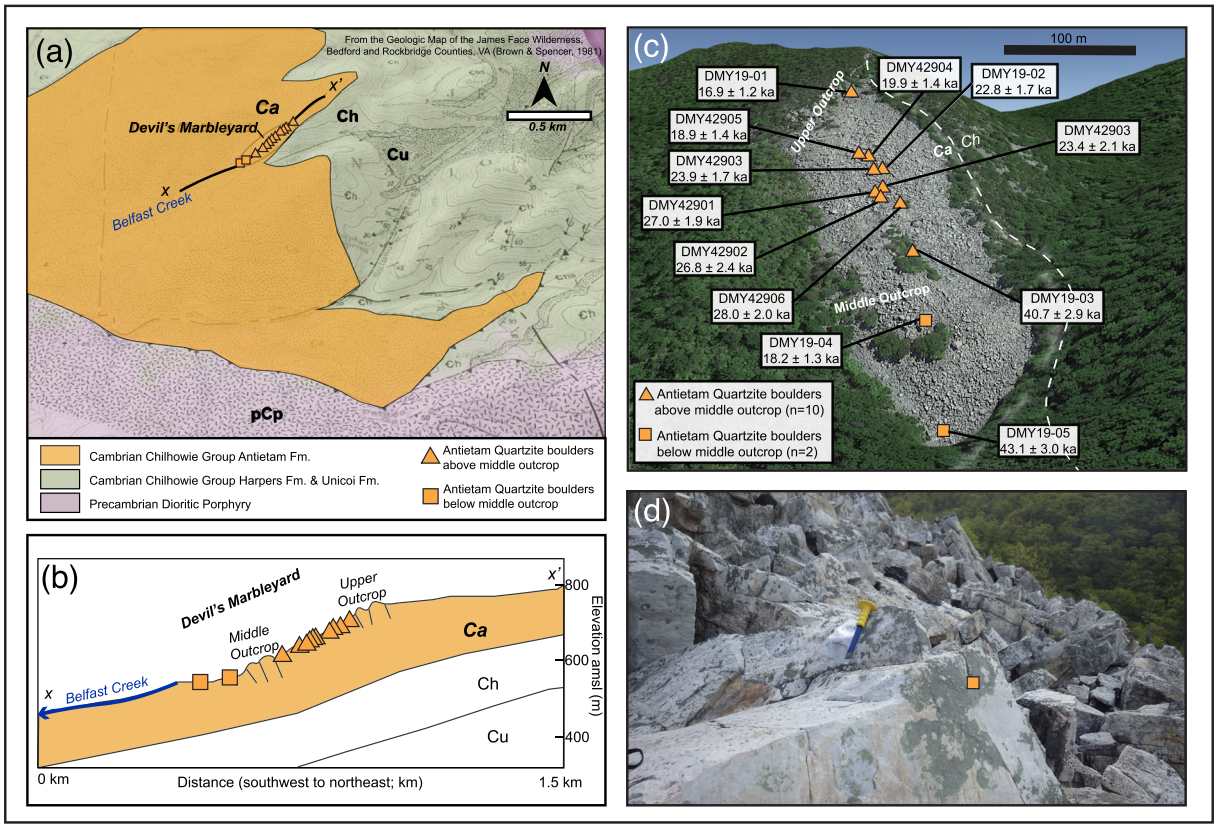

FIGURE 5 (a) The geologic setting for Devil's Marbleyard study area from the Geologic Map of the James River Face Wilderness, Bedford and Rockbridge Counties, VA (Brown & Spencer, 1981), includes the following major bedrock units: Cambrian Chilhowie Group composed of the Antietam Formation (Ca) (the boulder forming unit), Harpers Formation (Ch) and Unicoi Formation (Cu) and a Precambrian Dioritic porphyry. (b) The Devil's Marbleyard geology shown in cross section from x-x′ with boulder sample sites included at the surface separated out as those sampled above the middle outcrop (triangles) and below the middle outcrop (squares). (c) Google Earth Imagery of the Devil's Marbleyard boulder field study area in the Virginia Blue Ridge with sample sites and cosmogenic ages labelled. The dashed white line separates Chilhowie Group Antietam Formation (Ca) from the Harpers Formation (Ch). Samples collected above the middle outcrop ($n = 9$) are represented by triangle markers; these samples' likely source is the upper outcrop. Samples located below the middle outcrop ($n = 2$) are shown as square markers; the middle outcrop is the likely source of these boulders. There is a trend between distance downslope from outcrop source and boulder exposure age. (d) Example photograph of Devil's Marbleyard from the centre of the boulder field. For annotated photographs of all sampled boulders, see Figure S2.

process can operate in unconfined, non-saturated environments and across a broad range of subfreezing temperatures (Girard et al., 2013; Murton et al., 2006; Walder & Hallet, 1985, 1986). Though wetter substrates may be able to generate greater fracture intensity (Girard et al., 2013; Sass, 2005), water is usually not the limiting factor. Rather, MAAT and ATA exert a dominant control on segregation ice growth. The specific MAAT and ATA at which ice segregation can do appreciable damage to rocks are dependent upon the critical strength, porosity, permeability, and cohesion of the host rock or soil and will therefore be distinct in different lithologies and environments (Krautblatter et al., 2012; Marshall et al., 2021; Murton et al., 2006; Rempel et al., 2016; Walder & Hallet, 1985). Generally, more resistant rocks require a colder upper boundary of MAAT and/or a larger ATA to cause frost cracking. As temperatures get too cold, ice segregation growth ceases because supercooled water freezes in pore spaces causing a decrease in porosity and permeability; this sets the lower temperature bounds for frost cracking (Rempel et al., 2016).

A model of frost cracking intensity across unglaciated North America during the LGM indicates that the Virginia Blue Ridge and Valley and Ridge provinces experienced porosity increases as high as 0.34 mm annually down to depths of ~2 m because of frost cracking (Marshall et al., 2021). In addition to boulder deposits, other relict morphologic features, such as patterned ground, terraces, and large alluvial fan systems, across the mid-Atlantic and southern Appalachians have been assigned an origin tied to periglacial processes (Clark & Ciolkosz, 1988; Marsh, 1987; Merritts & Rahnis, 2022; Potter & Moss, 1968; Whittecar & Ryter, 1992). Recent work from Pennsylvania using geochronology suggests that Appalachian periglacial features may be multigenerational in origin, persisting through multiple Quaternary glacial stages (e.g., Del Vecchio et al., 2018; Denn et al., 2018). In older studies, a lack of access to reliable means of dating periglacial features often encouraged an unconstrained allocation of their origin to the LGM. For example, in the Virginia Valley and Ridge province, boulder deposits from Little Stony Creek (Figures 2 and 4) have long been observed and speculated over as an LGM periglacial feature (Mills, 1981, 1989), but the timing of deposition, post-depositional stability, mechanism of formation and landscape-scale geomorphic function of these features have yet to be fully determined and considered together.

TABLE 1 ^{10}BE DATA for boulder samples.

Sample	Location °N/°W	Elevation (m amsl)	Stratigraphic unit	Stratigraphic age	Dimensions (L × W × H; m)[a]	Depth (cm)[b]	Shielding factor[c]	SiO_2 (g)	^{9}Be carrier (mg)	^{9}Be carrier conc. (ppm)	^{10}Be (10^5 atoms g^{-1})[d]	Age (ka)[e,f,g,h]
Brush Mountain												
BRUSH19-02	37.27277/-80.44918	745	Cloyd	Mississippian	3 × 2.5 × 3	5	0.983901	20.0582	0.2033	0.961	3.25 ± 0.08	51.8 ± 3.6
BRUSH19-03	37.27291/-80.44933	733	Cloyd	Mississippian	5 × 3 × 1.5	5	0.993514	20.0124	0.2013	0.961	4.48 ± 0.08	73.4 ± 4.9
BRUSH21–01	37.27328/−80.45000	738	Cloyd	Mississippian	4 × 3 × 3	3	0.997701	20.0067	0.2037	0.961	2.29 ± 0.05	35.2 ± 2.4
Gap Mountain												
GAP19-02	37.27919/-80.48628	763	Keefer	Silurian	5 × 4 × 2	5	0.983811	20.0262	0.2066	0.961	3.62 ± 0.07	57.0 ± 3.8
GAP21-01	37.27973/-80.48465	741	Tuscarora	Silurian	5 × 4 × 2	2	0.986758	20.0302	0.2033	0.961	1.94 ± 0.05	29.8 ± 2.0
GAP21-02	37.27861/-80.48835	782	Keefer	Silurian	5 × 4 × 2	2	0.977018	20.0034	0.2027	0.961	1.74 ± 0.04	26.2 ± 1.8
GAP21-03	37.27897/-80.48908	811	Keefer	Silurian	5 × 4 × 4	4	0.974615	20.0045	0.2061	0.961	1.57 ± 0.04	23.6 ± 1.6
GAP21-04	37.27802/-80.48812	761	Tuscarora	Silurian	7 × 2.5 × 1.5	1	0.987368	19.9999	0.2046	0.961	6.66 ± 0.02	101.7 ± 6.9
Little Stony Creek												
LSC19-01	37.35422/-80.59711	694	Tuscarora	Silurian	11 × 5 × 6	4	0.969789	19.9777	0.2007	0.961	4.66 ± 0.01	77.9 ± 5.4
LSC19-02	37.35831/-80.58871	746	Tuscarora	Silurian	5 × 3 × 1	5	0.946272	20.1264	0.2044	0.961	1.93 ± 0.06	31.5 ± 2.2
LSC19-03	37.35852/-80.58846	746	Tuscarora	Silurian	9 × 6 × 3	5	0.943764	11.3197	0.2036	0.961	1.03 ± 0.05	16.9 ± 1.3
LSC19-04	37.35847/-80.58836	743	Tuscarora		6 × 4 × 2	5	0.942060	20.0018	0.2049	0.961	0.66 ± 0.03	10.8 ± 0.8
Devil's Marbleyard												
DMY19-01	37.58181/-79.47069	705	Chilhowie	Cambrian	2 × 1.5 × 2.5	5	0.978590	19.9732	0.2031	0.961	1.04 ± 0.04	16.9 ± 1.2
DMY19-02	37.58107/-79.47194	645	Chilhowie	Cambrian	4 × 4 × 2	5	0.977933	20.0141	0.2037	0.961	1.34 ± 0.05	22.8 ± 1.7

(Continues)

TABLE 1 (Continued)

Sample	Location °N/°W	Elevation (m amsl)	Stratigraphic unit	Stratigraphic age	Dimensions (L × W × H; m)[a]	Depth (cm)[b]	Shielding factor[c]	SiO_2 (g)	^{9}Be carrier (mg)	^{9}Be carrier conc. (ppm)	^{10}Be (10^5 atoms g^{-1})[d]	Age (ka)[e,f,g,h]
DMY19-03	37.58054/-79.47285	586	Chilhowie	Cambrian	3.5 × 2.5 × 3.5	5	0.983423	20.0438	0.2077	0.961	2.27 ± 0.07	40.7 ± 2.9
DMY19-04	37.58031/-79.47337	573	Chilhowie	Cambrian	4 × 2 × 3	5	0.984995	20.0106	0.2032	0.961	1.01 ± 0.04	18.2 ± 1.3
DMY19-05	37.58006/-79.47387	538	Chilhowie	Cambrian	3 × 2 × 1.5	5	0.976896	20.0052	0.2048	0.961	2.31 ± 0.06	43.1 ± 3.0
DMY42901	37.58100/-79.47220	625	Chilhowie	Cambrian	L = 2–5 m[i]	5	0.983648	16.7490	0.2658	1.000	1.66 ± 0.05	28.8 ± 2.1
DMY42902	37.58100/-79.47220	625	Chilhowie	Cambrian	L = 2–5 m[i]	5	0.983648	17.4550	0.2686	1.000	1.56 ± 0.04	27.0 ± 1.9
DMY42903	37.58109/-79.47196	636	Chilhowie	Cambrian	L = 2–5 m[i]	5	0.978147	16.9390	0.2681	1.000	1.39 ± 0.05	23.9 ± 1.7
DMY42904	37.58118/-79.47182	647	Chilhowie	Cambrian	L = 2–5 m[i]	5	0.976377	18.6990	0.2680	1.000	1.17 ± 0.04	19.9 ± 1.4
DMY42905	37.58124/-79.47183	647	Chilhowie	Cambrian	L = 2–5 m[i]	5	0.977708	15.5730	0.2671	1.000	1.11 ± 0.04	18.9 ± 1.4
DMY42906	37.58083/-79.47226	620	Chilhowie	Cambrian	L = 2–5 m[i]	5	0.984771	17.6550	0.2662	1.000	1.61 ± 0.05	28.0 ± 2.0

[a]Boulder dimensions: length (L) × width (W) × height (H) to nearest half metre.
[b]Depths sampled to the nearest cm; the tops of all samples were exposed at the surface.
[c]Shielding correction for topography was calculated using the shielding model from Li (2018) and a 1 arc-second DEM. A value of 1.0000 indicates no shielding.
[d]One-sigma AMS uncertainty.
[e]Calculated using the calculator formerly known as CRONUS Earth (http://hess.ess.washington.edu/) (Balco et al., 2008) using the Balco et al. (2009) Northeastern North America (NENA) production rate and 'St.' scaling from Stone (2000), which is based on Lal (1991).
[f]An assumed denudation rate of 0 mm yr^{-1} was used in all calculations.
[g]An assumed density of 2.7 g cm^{-3} was used in all calculations.
[h]Samples normalized to standard Be-01-5-4 with an assumed ^{10}Be/^{9}Be ratio of 2.851 × 10^{-11} (Nishiizumi et al., 2007).
[i]Boulder dimensions measured for an undergraduate thesis were not recorded beyond an estimate of long axis range (L).

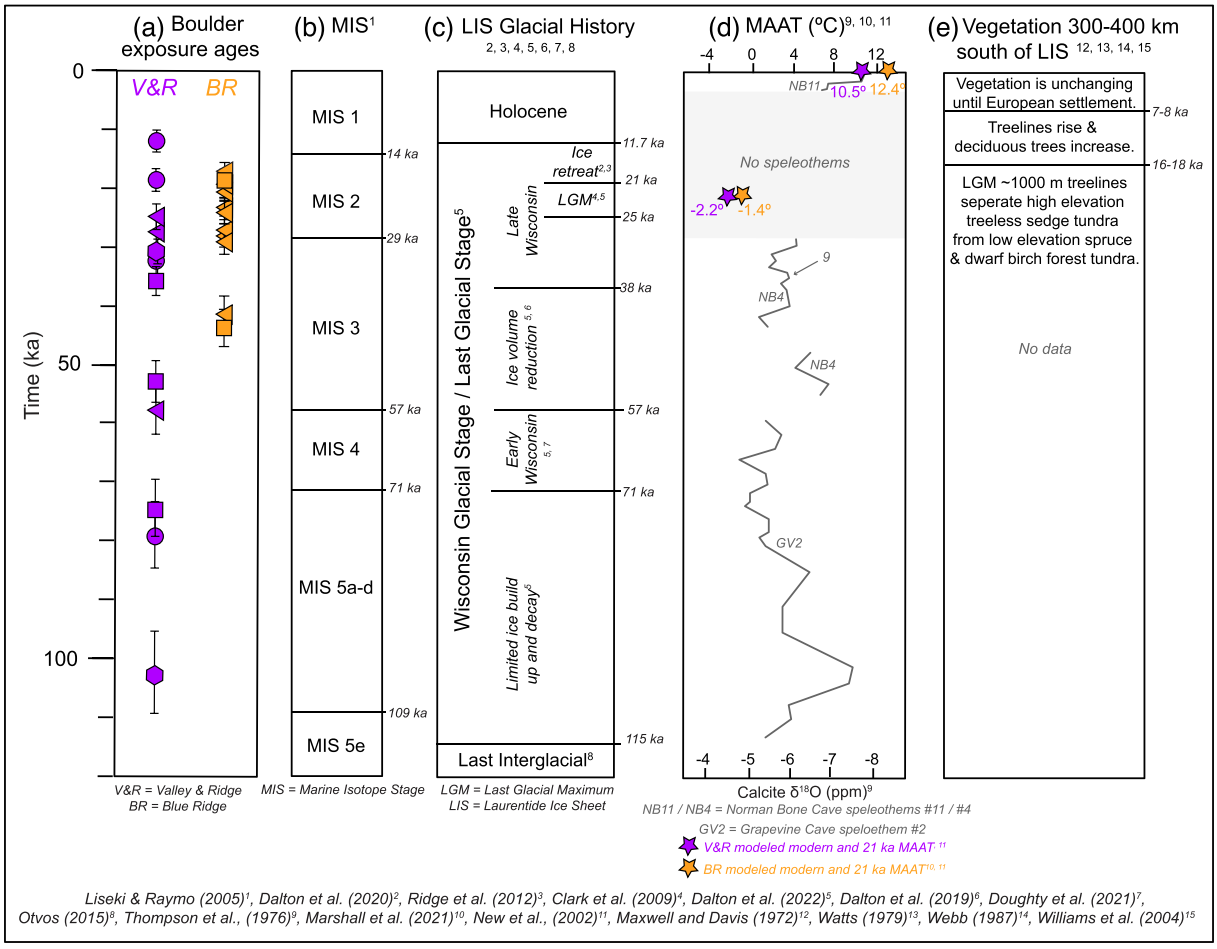

FIGURE 6 (a) Valley and Ridge (purple) and blue Ridge (orange) boulder exposure ages (specific symbology defined in Figures 3–5 and 7) are plotted from 120 ka through the present. (b) Marine Isotope Stages (MIS) (Lisiecki & Raymo, 2005), though not a perfect representation of ice volume, are presented as a useful climate chronology framework. (c) This panel shows a summary of the glacial history of the Laurentide Ice Sheet (LIS) from 120 ka through the present (Carlson et al., 2018; Clark et al., 2009; Dalton et al., 2019, 2020, 2022; Doughty et al., 2021; Otvos, 2015; Ridge et al., 2012). (d) The speleothem climate proxy of Thompson et al. (1976) is from Norman Bone Cave and Grapevine Cave, West Virginia, located ~70–90 km north/northwest of our study sites (locations shown in Figure 2). This record is derived from the analysis of several formations covering different age ranges including Grapevine Cave Flowstone 2 (GV2), Norman Bone Cave Stalagmite 4 (NB4), Norman Bone Cave Stalagmite 10 (NB10) and Norman Bone Cave Stalagmite 11 (NB11). The grey-shaded box indicates a major gap in the speleothem record. Stars indicate modelled modern and 21 ka MAAT (values from Figure 1; Marshall et al., 2021; New et al., 2002). (E) Summarized vegetation history in our study area from the LGM through the European settlement is based on fossil and pollen work (Maxwell & Davis, 1972; Watts, 1979; Webb, 1987; Williams et al., 2004).

2.3 | Regional glacial and periglacial history

Although Marine Isotope Stages (MIS) (Lisiecki & Raymo, 2005) cannot be interpreted directly as proxies for regional glacial ice volumes or terrigenous temperature, they do provide a useful and globally correlated chronologic framework through which to view climatic events. As such, we name correlative MIS along with regional glacial reconstructions and nomenclature in our discussion of the glacial and periglacial history of our study area, even though correlations between the two are not exact (Figure 6b).

The Laurentide Ice Sheet (LIS) has advanced and retreated repeatedly across north-eastern North America throughout the Quaternary to the north of our study areas (e.g., Dyke, 2004) (Figure 1). The penultimate Illinoian Glacial Stage of the LIS occurred between 191 and 130 ka (MIS 6) and was followed by warming and glacial retreat during the Last Interglacial Stage (Sangamon) between 130 and 115 ka (~MIS 5e) (Otvos, 2015). During the Last Glacial Stage, the Wisconsin Glacial Stage in North America (~115–10 ka or ~MIS 5d—MIS 2), the LIS was the largest ice mass to grow and then retreat on the planet (Dalton et al., 2022; Otvos, 2015) (Figure 6c). Although the exact extent of the LIS during the early parts of the Wisconsin Glacial Stage are highly speculative, Dalton et al. (2022) suggests a period of limited ice build-up and then retreat between 115 and 80 ka (~MIS 5a–d; Figure 6b,c). During the Early Wisconsin advance, between ~71 and 57 ka (~MIS 4), LIS ice volume expanded and was at its largest (just below LGM volumes) by 60 ka (Dalton et al., 2022; Doughty et al., 2021). There is evidence for a dramatic reduction in the size of the LIS between ~52 and 40 ka (early MIS 3) such that its limits were north of the Hudson Bay Lowlands (Dalton et al., 2019). The MIS 3 retreat was followed by the onset of the LIS advance towards its LGM extent in the late Wisconsin starting between 38 and 35 ka and reaching full LGM conditions between 29 and 25 ka (middle MIS 3 through MIS 2) (Carlson et al., 2018; Dalton et al., 2022). LGM ice limits stayed at or near their maximum extent until the LIS began its

retreat between 24 and 21 ka. Full interglacial conditions were achieved by the beginning of the Holocene (11.7 ka; early MIS 1) (Clark et al., 2009; Dalton et al., 2020; Ridge et al., 2012).

During advances of the LIS, periglacial conditions persisted in a broad swath of land south of the glacial limits. Periglacial environments are non-glaciated environments with deep frozen ground that either returns seasonally or persists through multiple years (Ballantyne, 2011; French, 2017; Lowe & Walker, 2015; Marshall et al., 2021; Merritts & Rahnis, 2022). When the LIS was at its LGM extent, periglacial conditions extended from the ice-sheet margin in Pennsylvania to Georgia. Discontinuous permafrost (permafrost which covers 50–90% of the land area) occupied broad areas directly proximal to the ice sheet as well as higher elevations portions of the Appalachian Mountains as far south as the state of Georgia (Lindgren et al., 2016). The Virginia Appalachians, located ~350 km south of the limits of the LIS during the LGM, were never glaciated but repeatedly experienced periglacial climatic conditions (Figure 1) with modelled local average winter temperatures as low as −10°C during the LGM (Shafer et al., 2021).

Pollen and fossil datasets suggest that south of LIS while it was at its LGM extent up through ~17–18 ka, the spatial distribution of vegetation types was consistent (Figure 6e). During this time, treeless sedge tundra, similar to what occurs in the modern Arctic, was present at all elevations within ~60 km of the ice-sheet margin and at high elevations in a swath of land ~300–400 km south of the ice sheet (Watts, 1979; Webb, 1987; Williams et al., 2004). In the Shenandoah region of Virginia, just north of our study area, the tree line separating sedge tundra from forest tundra is estimated to have been at an elevation of ~1,000 m amsl (Maxwell & Davis, 1972). Forest tundra containing spruce and dwarf birch persisted at lower elevations, including our study areas (538–811 m amsl). During LIS deglaciation and into the early Holocene, vegetation changed nearly continuously from ~16 to ~8 ka as the ice sheet was retreating (Webb, 1987; Williams et al., 2004). Dwarf birch and spruce expanded into the former sedge tundra regions, tree lines rose across the Appalachians, and former pine forests had increasing proportions of deciduous trees including oak and hazel, all indicating warming climate conditions (Maxwell & Davis, 1972). Vegetation types remained relatively consistent between 7 ka and 500 years BP, when European settlement and land use changes drove renewed shifts in vegetation patterns in eastern North America (Williams et al., 2004) (Figure 6e).

2.4 | Local paleo-temperature estimates

LGM MAAT at 21 ka, estimated from the ensemble climate model of Marshall et al. (2021), is −1.4°C in the Blue Ridge study area and −2.2°C in the Valley and Ridge study area (Figure 1b). ATA at 21 ka, also estimated from the ensemble climate model is 14.3°C in both the Blue Ridge and Valley and Ridge study areas (Figure 1d). Modern MAAT is estimated as 12.4°C in the Blue Ridge study area and 10.5°C in the Valley and Ridge study area (Figure 1a) (Marshall et al., 2021; New et al., 2002). Modern ATA is 11.4°C in the Blue Ridge study area and 11.3°C in the Valley and Ridge study area (Figure 1c) (Marshall et al., 2021; New et al., 2002).

Stable isotope geochemistry and geochronology of speleothems from Norman Bone and Grapevine Caves from the Appalachian Plateau of West Virginia, located ~70–90 km northwest of our study sites (Figure 2), are the closest record of regional late Quaternary terrigenous paleoclimate to our study areas (Thompson et al., 1976). There are significant gaps in the West Virginia speleothem record that have been interpreted as times when conditions were too cold or too dry for speleothem growth, but it is also possible that they are missing because of preservation issues. The pattern (though not absolute values) of MAAT changes derived from the speleothem record is consistent with what might be expected based on LIS glacial reconstructions and the MIS records of global temperature, with one exception (Figure 6). That exception is the ~100 ka peak in temperature (Figure 6d), which is as warm as modern estimates of MAAT. This apparent peak in temperature post-dates the Last Interglacial by ~10–15 ka. Whether this offset is real or a geochronology problem is beyond the scope of the study but should be carefully considered when using the Thompson et al. (1976) temperature record to consider climate condition in the earliest Wisconsin (~MIS 5a–d).

3 | METHODOLOGY AND METHODS

We measured the concentration of ^{10}Be in quartz from the upper surfaces of 23 large boulders in the Valley and Ridge and Blue Ridge study areas and then calculated exposure ages to constrain the timing of boulder deposition. Cosmic ray particles derived from nuclear reactions in the atmosphere produce *in situ* cosmogenic nuclides in target minerals as they pass through the top few metres of soil, sediment and rock (Dunai & Lifton, 2014; Gosse & Phillips, 2001; Lal, 1991). The concentration of ^{10}Be in the target mineral quartz (atoms ^{10}Be g^{-1}) has widely been used to investigate the timing and rates at which a variety of geomorphic processes operate (Brown et al., 1995; Hancock et al., 1999; Nishiizumi et al., 2007; Portenga & Bierman, 2011; Staiger et al., 2006; Ward et al., 2005). The production rate of ^{10}Be at depth (atoms ^{10}Be g^{-1} $year^{-1}$) is dependent upon a regional surface production rate, sample depth and decay length scale ($z^* = \Lambda/\rho$ where ρ = rock density and Λ = attenuation length of 160 g cm^{-2}) (Bierman, 1994; Hancock et al., 1999; Lal, 1991; Lal et al., 1996; von Blanckenburg & Willenbring, 2014). In the simplest case, the ^{10}Be concentration sampled from the upper surface of a boulder should be a function of time of exposure at the surface, sample depth and the ^{10}Be decay constant ($\lambda = \ln 2/t_{1/2}$; yr^{-1}) where the half-life ($t_{1/2}$) for ^{10}Be is 1.386 ± 0.016 My (Chmeleff et al., 2010). In this study, we interpret ^{10}Be exposure ages to constrain the time elapsed since boulder deposition.

We conducted quartz cleaning, sample spiking with ^{9}Be and the isolation of beryllium at the Dartmouth College Cosmogenic Laboratory and sent samples to the Purdue Rare Isotope Measurement Laboratory (PRIME Lab) at Purdue University for Accelerator Mass Spectrometry (AMS) measurements of ^{9}Be/^{10}Be ratios. Exposure ages were calculated from ^{10}Be concentrations using what was formerly known as the CRONUS Earth online calculator (Balco et al., 2008) using an assumed erosion rate of 0 cm $year^{-1}$ and a rock density of 2.7 g cm^{-3}. The assumed 0 cm $year^{-1}$ erosion rate means that our calculated exposure ages are minimum ages. We used the Northeastern North America (NENA) production rate calibration (Balco et al., 2009) and time-independent scaling ('St') of Lal (1991) and Stone (2000). Topographic shielding of ^{10}Be production was

accounted for using a shielding factor calculated for each sample using the methods of Li (2018) from a 1-arc sec digital elevation model (Table 1).

To interpret exposure ages as the amount of time that has passed since boulders were deposited on the hillslope after being detached from bedrock, we must assume no significant pre-existing concentration (i.e., 'inheritance') of ^{10}Be in boulder surfaces and no change in the orientation of the top surface of the boulder due to post-depositional rolling. To minimize the possibility of inheritance, boulders were visually inspected on all sides and only selected for dating if the top surface was not weathered significantly more than the other sides of the boulder; the goal being to avoid dating boulder surfaces coincident with the previous outcrop surface, which would likely have the most inheritance. To minimize the possibility of rolling since deposition, only large boulders (whose shortest axis is >2 m) in a stable orientation (longest axis semi-parallel to the hillslope surface) were selected. All sampled boulders are tabular or blocky rather than round and therefore are not likely to roll once emplaced (Figure S3).

4 | RESULTS

In the Valley and Ridge study site, Brush Mountain conglomerate hillslope boulders from elevations of 733–745 m amsl ($n = 3$) have ^{10}Be concentrations ranging from 2.29 ± 0.05 × 10^5 to 4.48 ± 0.08 × 10^5 atoms ^{10}Be g^{-1} and calculated exposure ages between 35.2 ± 2.4 and 73.4 ± 4.9 ka (Table 1 and Figure 3). Gap Mountain sandstone hillslope boulders from elevations of 741–811 m amsl ($n = 5$) have ^{10}Be concentrations ranging from 1.57 ± 0.04 × 10^5 to 6.66 ± 0.02 × 10^5 atoms ^{10}Be g^{-1} and calculated exposure ages between 23.6 ± 1.6 and 101.7 ± 6.9 ka (Table 1 and Figure 3). Little Stony Creek sandstone channel boulders from elevations of 694–746 amsl ($n = 4$) have ^{10}Be concentrations ranging from 0.66 ± 0.03 × 10^5 to 4.66 ± 0.01 × 10^5 atoms ^{10}Be g^{-1} and calculated exposure ages between 10.8 ± 0.8 and 77.9 ± 5.4 ka (Table 1 and Figure 4). Within the Valley and Ridge samples, no relationship exists between boulder exposure age and sample site elevation, lithology, boulder size, or boulder position (hillslope vs channel; Figure 7).

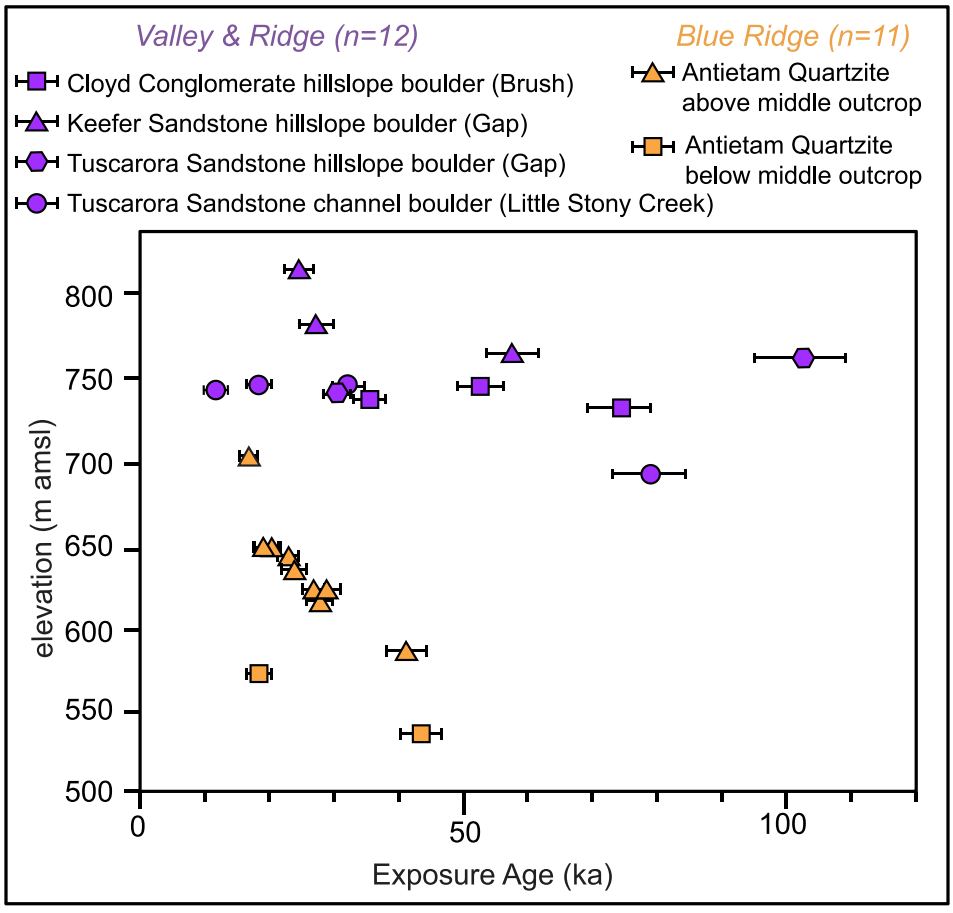

FIGURE 7 Exposure age versus elevation for all Valley and Ridge (purple) and Blue Ridge (orange) samples. Valley and Ridge sandstone and conglomerate boulders are from elevations of 694–811 m amsl ($n = 12$) and have ^{10}Be exposure ages, which range from 10.8 ± 0.8 ka to 101.7 ± 6.9 ka. Different lithologic unit and boulder types (hillslope vs. channel position) in the Valley and Ridge are represented by marker shapes; no relationship exists between boulder exposure age and elevation, lithology or boulder type. Blue Ridge quartzite boulder is from elevations of 538–705 m amsl ($n = 11$) and has exposure ages, which range from 16.9 ± 1.2 ka to 43.1 ± 3.0 ka. Blue Ridge marker shapes differentiate between samples deposited above the middle outcrop (whose likely source is the upper outcrop) and those from and below the middle outcrop (whose likely source is the middle outcrop; see Figure 5). Assuming this division in source outcrop, Blue Ridge boulder exposure ages increase with downslope distance from source rock. A comparison between the two groups indicates that higher elevation sedimentary boulders from the Valley and Ridge have a broader range of exposure ages than lower elevation quartzite boulders from the Blue Ridge.

In the Blue Ridge sample site at Devil's Marbleyard, quartzite boulders from elevations of 538–705 m amsl ($n = 11$) have ^{10}Be concentrations ranging from $1.04 \pm 0.04 \times 10^5$ to $2.31 \pm 0.06 \times 10^5$ atoms ^{10}Be g^{-1} and calculated exposure ages between 16.9 ± 1.2 and 43.1 ± 3.0 ka (Table 1 and Figure 5). At Devils Marbleyard, boulder position on the hillslope relative to bedrock outcrops indicate an upper outcrop as the most likely source for nine of the highest elevation samples and a middle outcrop as the most likely source for the lower two boulders (Figure 5b,c). Assuming this division in source outcrop, Blue Ridge boulder exposure ages increase with downslope distance from source rock (Figure 7).

5 | DISCUSSION

5.1 | Boulder exposure ages within a climate framework

Out of 23 measured boulder exposure ages, 22 correspond to the Wisconsin Glacial Stage and subsequent LIS deglaciation (between 115 and 11.7 ka, Figure 6a,c). The one remaining age, LSC19-04 (10.8 ± 0.8 ka), corresponds to the earliest Holocene. Although LSC19-04 postdates major LIS retreat, it still fits within the 17–7 ka window of time following LIS retreat when the southern Appalachians were still experiencing major vegetation changes following ice retreat including rising tree line elevations and increasing proportions of deciduous tree (Figure 6e). The correlation between measured boulder exposure ages and the Wisconsin Glacial Stage suggests a periglacial origin for large hillslope and channel boulders in the Virginia Appalachians but does not confirm a process by which boulders were detached and deposited.

Enhanced frost cracking of ridge bedrock is a possible process by which periglacial conditions could result in the deposition of large boulders. All exposure ages, except the oldest sample, GAP21-04 (101.7 ± 6.9), correspond to times when the speleothem climate records from West Virginia (Thompson et al., 1976) indicate regional MAAT was ≤8°C (Figure 6d) and model predicted ATA corresponding to this time interval ranged from 11.3–14.3°C (Marshall et al., 2021). Gap 21-04 may also have formed within this temperature range if the speleothem geochronology is problematic as inconclusively discussed in Section 2.4. The phase diagram from Marshall et al. (2021), which predicts annual porosity change due to frost cracking (mm) as a function of MAAT and ATA, predicts that under these conditions there would be ~0.34–0.08 mm of porosity change due to frost cracking per year (Figure S4). This suggests that frost cracking is a physically possible mechanism for the fracturing of bedrock, detachment and deposition of the boulders dated in this study.

Another periglacial condition that might result in the deposition of large boulders is decreased stabilization of ridge bedrock because of decreases in large trees, other vegetation and soil under a periglacial climate (Figure 6e). Prior work supports the presence of forest tundra conditions in our field areas during LIS advances throughout the Wisconsin Glacial Stage with smaller and fewer trees and decreased soil production (Maxwell & Davis, 1972; Watts, 1979; Webb, 1987; Williams et al., 2004). Further supporting this idea is the observation that some boulder producing units, such as the Cloyd Conglomerate, do not outcrop regularly at the surface today under Holocene climatic conditions upslope from the deposits. Rather, soil and plants have infilled and stabilized these outcrops indicating the need for very different soil and plant conditions during times of rock detachment and boulder deposition (Figure S3).

5.2 | What about the ages that are not there?

While the absence of certain exposure ages in our dataset does not preclude boulder deposition during those times, it does at least suggest that they are less prevalent and thus missed in the course of sampling. In both the Valley and Ridge and Blue Ridge field areas, there are no boulder exposure ages from the Last Interglacial Stage (Sangamon) or from the warmest last 10 ka of the Holocene. This suggests that during interglacial and postglacial times, there is no significant mechanism by which large boulders are deposited on hillslopes and in channels. Boulders sampled directly adjacent to source outcrops yield ages of ~17–18 ka at Devils Marbleyard and ~24–26 ka at Gap Mountain, so the lack of post-glacial ages does not seem to be a result of a sampling bias towards boulders farther from the source outcrop that may have had more opportunity to move following detachment. Additionally, at least in the Blue Ridge, the stabilization of outcrops by interglacial soils and plants (Figure S3) does not support the likelihood of recent boulder detachment. The persistence of boulders with exposure ages correlating to the Wisconsin Glacial Stage suggests that throughout the Holocene, boulders armouring hillslopes and channels have been largely immobile. However, it is possible that the boulders have been very slowly weathering in place (as fits their resistant lithology), sluggishly creeping downslope in their original depositional orientation, or were occasionally dislodged by rare stochastic storm events.

One possible refutation to the argument of inter-/post-glacial boulder stability on the landscape is that the gap in measured boulder ages from the Wisconsin Glacial Stage is similar in duration to the most recent post-glacial (i.e., Holocene) gap in boulder exposure ages. For example, the ~15.5 ka age gap in our Valley and Ridge dataset between samples GAP19-02 (57.0 ± 3.8) and BRUSH19-03 (73.4 ± 4.9) is even longer than the gap between the youngest measured boulder age and the present (~10 ka). Despite this observation from the earlier part of the Wisconsin Stage, we do have continuous boulder exposure ages without any gaps, which correspond to the most recent late Wisconsin LIS advance (mid-MIS 3 through MIS 2, ~38 ka through LGM; Figure 6) from both the Blue Ridge and Valley and Ridge study sites. This at least supports boulder stability since the most recent Wisconsin LIS advance and corresponding periglaciation. Still, collecting more samples would be the only way to get a better picture of whether these are truly gaps in boulder deposition or if they are just a product of the limited sample size.

Looking deeper in time, no boulder ages are from the Illinoian or older Quaternary glacial stages. One interpretation of the lack of boulder ages from earlier glaciations might be that it suggests something special about conditions during the Wisconsin Glacial Stage for the deposition of periglacial boulders (Figure 8a). However, given that temperature conditions during older glacial times were comparably as cold as the Wisconsin Stage (Lisiecki & Raymo, 2005; Thompson et al., 1976), such an explanation seems unlikely. An alternative

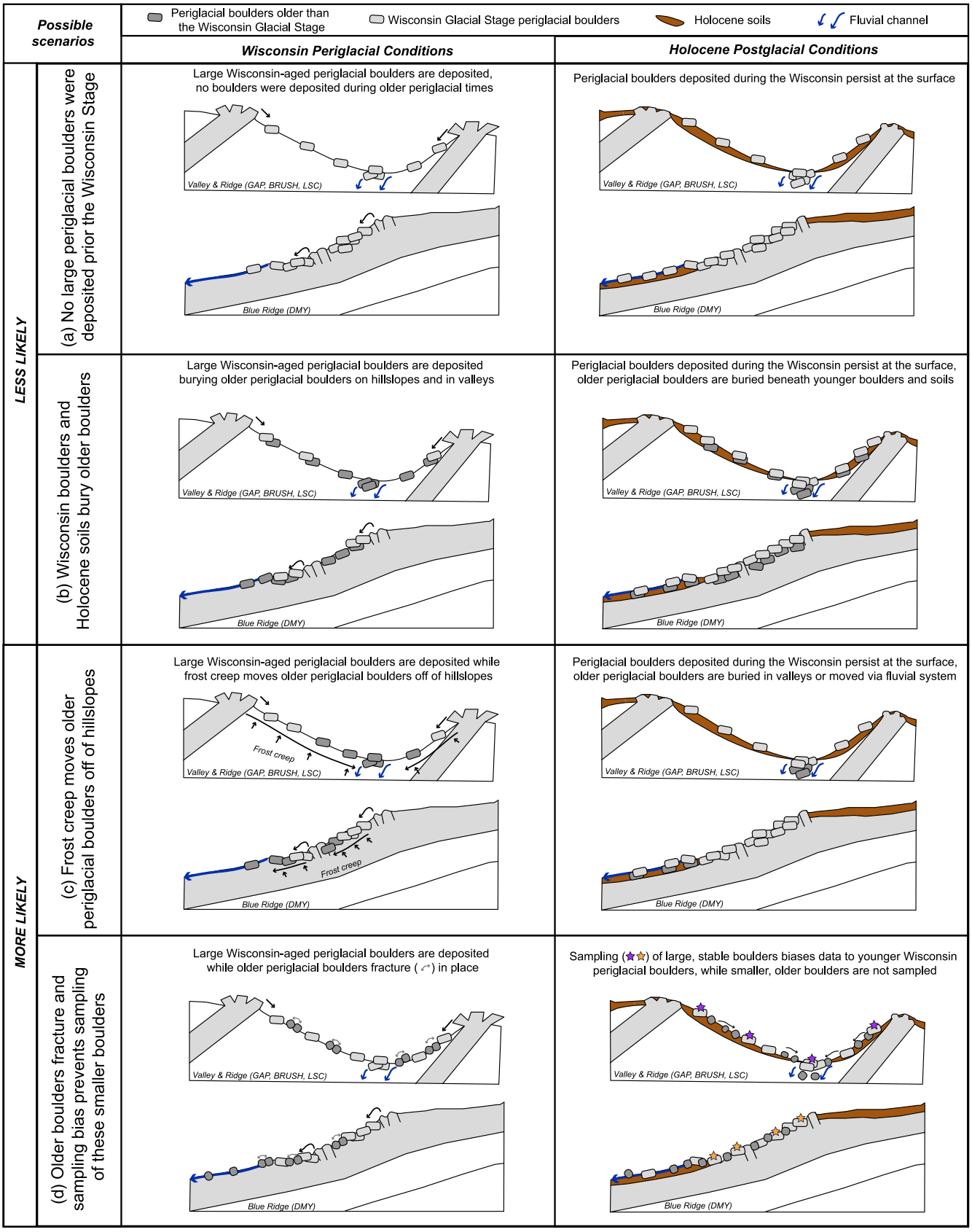

FIGURE 8 Legend on next page.

FIGURE 8 In panels (a)–(d), we illustrate four possible end-member scenarios that could result in Wisconsin-aged boulder exposure ages. Dark grey blocks represent periglacial boulders deposited during Illinoian or older glacial advances (i.e., pre-Wisconsin periglacial boulders), times that did not yield any exposure ages in this study, allowing us to explore possible fates of these boulders. Light grey blocks represent boulders deposited during the Wisconsin Glacial Stage, which did yield exposure ages in this study. Blue arrows indicate the location of modern-day fluvial channels. The left column shows the idealized Valley and Ridge (top in each panel) and Blue Ridge (bottom in each panel) study areas in cross section during the Wisconsin Glacial Stage, when periglacial conditions persisted. The right column shows the idealized Valley and Ridge (top in each panel) and Blue Ridge (bottom in each panel) study areas during the Holocene up through the time of sampling, when post-glacial conditions persisted. In all scenarios, only large, Wisconsin-aged boulders are exposed at the surface in the Holocene, supported by our results. We consider scenarios (a), no large periglacial boulders deposited prior to the Wisconsin stage, and (b), Wisconsin boulders and Holocene soils bury older boulders, to be less likely because similarly cold periglacial conditions occurred during glacial stages preceding the Wisconsin and because it is unlikely that net deposition is occurring over long timescales due to steep headwater streams at the base of the hillslopes. We consider scenarios (c), frost creep moves older periglacial boulders off hillslopes; (d), older boulders fracture and sampling bias prevents sampling of these smaller boulders; or some combination of scenarios (b)–(d), to be the more likely based on climatic conditions and field evidence of boulder deposits.

interpretation is that boulders were deposited on hillslopes and channels during penultimate and older periglacial times, but surface processes caused hillslopes and channels to be resurfaced with large boulders with each return to periglacial conditions. Perhaps older periglacial boulders are buried beneath younger periglacial boulders and post-/interglacial soils (8B). Such a scenario seems possible over short timescales as a means of intermittent sediment storage but less likely over longer timescales, such as multiple glacial–interglacial cycles. Long timescales of burial imply a net depositional setting and the presence of steep headwater streams at the base of hillslopes points towards these regions undergoing net erosion. More likely scenarios by which hillslope processes could resurface the landscape include older periglacial boulders being moved off hillslopes under recent periglacial conditions via frost creep processes (Andersen et al., 2015; Figure 8c) or broken down by in situ frost cracking into smaller boulders, which could be moved out of catchments through fluvial systems or which would not be selected for exposure dating based on their size (Figure 8d). Some combination of these nonunique endmember scenarios or others not considered here may be possible mechanisms for hillslope and channel resurfacing.

5.3 | Differences between Valley and Ridge and Blue Ridge boulder ages

The distribution of boulder exposure ages from the two geologic provinces has some significant and informative differences. Exposure ages from the boulders sampled at Devil's Marbleyard in the Blue Ridge province (16.9 ± 1.2 to 43.1 ± 3.0 ka; Figure 6a) have younger and more closely grouped exposure ages as compared to boulders from the Valley and Ridge province (10.8 ± 0.8 to 101.7 ± 6.9 ka; Figure 6a), which have a broader range of exposure ages that extend further back in time. At Devil's Marbleyard, 9 out of 11 exposure ages correspond to the most recent Late Wisconsin LIS advance (~38 ka through LGM; Figure 6). In the Valley and Ridge, exposure ages are spread out across the entirety of the Wisconsin Glacial Stage and through the earliest Holocene, though there is a higher concentration of exposure ages (6 out of 11) corresponding to the most recent late Wisconsin LIS advance (~38 ka through LGM; Figure 6). Below, we discuss several possible explanations for the differing distribution of ages between the two geologic provinces including (1) elevation and lapse rate controlled climatic conditions, (2) differences in rock strength and (3) differences in geomorphology and post-depositional hillslope processes.

Valley and Ridge boulders were sampled from elevations of 694–811 m amsl, while Blue Ridge boulders were sampled from a lower range of elevations between 538 and 705 m amsl. The ensemble climate model (Marshall et al., 2021), which uses a regional lapse rate to account for elevation's impact on temperature, indicates lower Valley and Ridge 21 ka MAAT (−2.2°C) and modern MAAT (10.5°C) as compared to the Blue Ridge 21 ka MAAT (−1.4°C) and modern MAAT (12.4°C; Figure 1a,b). A simple explanation for the difference in the range of boulder exposure ages in the Valley and Ridge versus Blue Ridge is that periglacial conditions persisted for a longer duration of the Wisconsin Glacial Stage at the higher elevation, colder Valley and Ridge sites as compared to the lower elevation, warmer site in the Virginia Blue Ridge.

Another interpretation of the difference in the spread of ages between the Valley and Ridge and Blue Ridge study sites is that it results from rock strength differences. Perhaps higher rock strength in the quartzite boulders of the Valley and Ridge as compared to the siliciclastic boulders of the Blue Ridge exerts a major control on the intensity of periglacial conditions required for frost cracking to drive boulder detachment from outcrops. Model predictions and lab experiments suggest that increased rock strength is correlated with the need for higher porosity change due to frost cracking (i.e., colder MAAT and higher ATA) to drive rock detachment (e.g., Rempel et al., 2016). No work exists that provides direct rock strength comparisons between the Valley and Ridge siliciclastic rocks and the Blue Ridge Antietam Quartzite sampled in this study, but we can use petrographic characteristics to make a first order comparison. A study from Hale and Shakoor (2003) found that 50 cycles of freezing and thawing decreased the unconfined compressive strength of a Pennsylvania sample of Tuscarora Sandstone from 14,224 to 9,878 psi. The same study considered the strength of a variety of other Appalachian sandstones in conjunction with their petrographic characteristics and found that in sandstones with a similar composition, unconfined compressive strength best correlates with the percentage of sutured and interlocking grain boundaries. The Tuscarora Sandstone has a very low porosity of <1% due to the omnipresence of secondary quartz cements and sutured grain contacts. Similarly, in a petrographic characterization of the Antietam Quartzite, Schwab (1970) suggests that the rock is classified as a quartzite, not due to heat-related recrystallization, but rather because of secondary silica cementation and quartz pressure solution driving the production of sutured grain boundaries. As the Tuscarora Sandstone and Antietam quartzite have similar compositions (>90% quartz) (Chilton & Spotila, 2020; Schwab, 1970) and share a characteristic interlocking quartz grain contact texture, it

seems unlikely that those two boulder source units have a significant difference in compressive strength.

Another factor to consider beyond rock compressive strength is the pre-existing weaknesses in rocks that can act as initiation sites for frost cracking. Extensive jointing in the Antietam Quartzite due to deformation during both Alleghenian thrusting and subsequent Mesozoic extension (Fichter et al., 2010) would, if anything, make the Antietam quartzite easier to fracture rather than more difficult. It seems more likely that the higher percentage of hillslope cover by boulders at Devils Marbleyard as compared to the Valley and Ridge sites might be attributed to the Antietam quartzite being easier to break because of its pre-existing brittle fractures rather than more difficult because of some intrinsic material property relating to compressive strength.

There are several major geomorphic differences between the Valley and Ridge and Blue Ridge and study regions. These geomorphic differences could explain the varying spread of surface exposure ages because of post-depositional hillslope processes without necessitating big differences in the conditions under which boulders were initially deposited. Percentage boulder cover in the Valley and Ridge is ≤9% on hillslopes and 20–90% in headwater channels, while percentage boulder cover at Devils Marbleyard is nearly 100%. The younger age range of boulders from Devil's Marbleyard might result from the higher likelihood that older boulders would be buried by younger boulders at least during the last glacial cycle (Figure 8b). Consequently, the lower percentage of hillslope cover in the Valley and Ridge means that it is less likely that older boulders would be completely covered by younger boulders during the last glacial cycle.

Mean hillslope angles in the Valley and Ridge study sites range from 12° to 18°, while the mean slope angle at Devils Marbleyard is 28°. A higher mean hillslope angle at Devils Marbleyard could correspond to a younger and tighter spread of ages because any boulders deposited under periglacial conditions corresponding to the early Wisconsin LIS advance (MIS4) might be more easily moved off hillslopes by frost creep processes under the most recent periglacial conditions (Figure 8c). The magnitude of sediment downslope movement via frost creep is based on the angular discrepancy between the magnitude of frost heave (parallel to the ground surface) and thaw settling (parallel to the force of gravity). For a given slope angle, frost creep transport proceeds with greatest efficiency when MAATs are close to freezing, driving the greatest frost heave magnitude. If frost heave magnitude is held constant, transport is most effective when hillslope angle is higher (Andersen et al., 2015). In the Valley and Ridge, lower slope angle could make downslope periglacial transport by frost creep less efficient leaving more older boulders on hillslopes though multiple LIS advances during the Wisconsin Stadial as compared to the Blue Ridge (Figure 8c).

5.4 | Comparison to Hickory Run Boulder Field, Pennsylvania

Hickory Run Boulder field in the Pennsylvania Appalachians is a nearly flat (slope = 1°), 550 × 150 m sandstone and conglomerate boulder field located ~2 km south of the LGM ice-sheet margin. In a study by Denn et al. (2018), ^{10}Be exposure ages from Hickory Run range from 70 to 600 ka. The exposure ages exhibit a trend of increasing age with distance downslope but are not correlated with boulder size or times of Quaternary glacial advances. One interpretation of the Hickory Run dataset is that boulder fields are long-lived features whose production is not necessarily tied to a single glacial stage, and which can persist through multiple glacial cycles. Another interpretation, based on the similarity between surface exposure time of Hickory Run Boulders and quartzite outcrops in the area (Portenga et al., 2013), is that these boulders are fracturing in place and yield ages that correspond to long term rock surface erosion rates both predating and postdating detachment from outcrop.

In contrast to our Virginia dataset of all Wisconsin Glacial Stage boulder surface exposure ages, the Hickory Run dataset pre-dated the Early and Late Wisconsin Stadials of the Last Glacial Stage. One possible explanation for the distinctive age ranges could be that when the LIS was at or near LGM extents during the Wisconsin Glacial Stage, Hickory Run was too close and thus too cold for significant frost cracking too proceed (Rempel et al., 2016). However, at Hickory Run 21 ka, MAAT is modelled as being −11.8°C and ATA as 13.3°C predicting 0.26 mm of annual porosity change due to frost cracking (Marshall et al., 2021). This suggests that frost cracking was a physically possible mechanism for boulder detachment at Hickory Run during near LGM climatic conditions.

Another possible explanation for the distinctive age ranges in the different settings is that they are a function of slope angle and the accompanying range of hillslope processes available to move boulders both upon initial detachment from outcrop and following deposition rather than a fundamental difference in the timing of bedrock fracturing and rock detachment. The higher mean slope condition in our study areas (from a low of 12° at Gap and Brush Mountain to 28° at Devil's Marbleyard), compared to 1° at Hickory Run, would allow for significant downslope movement of boulders immediately upon detachment and increased likelihood of exposing a fresh side of the newly formed boulder without significant inheritance upon deposition. Additionally, following initial deposition, higher hillslope angle could be responsible for differences in the rates of frost creep downslope boulder movement driving the resurfacing of hillslopes with new boulders during each return to periglacial conditions (Andersen et al., 2015). Perhaps there is a threshold average hillslope angle, somewhere between 1° (Hickory Run) and 12° (Gap and Brush Mountain), below which periglacial boulder fields are long lived multigenerational features and above which they experience a punctuated turnover and complete resurfacing with each return to periglacial conditions. As discussed above, the youngest and shortest age range from this study at Devil's Marbleyard has the highest slope angle, which might suggest that the rate at which boulder resurfacing occurs is positively related to hillslope angle.

5.5 | Implications of climatically punctuated boulder resurfacing in Appalachian landscapes

In previous work from these and other similar landscapes in the Virginia Appalachians (e.g., Chilton & Spotila, 2020; Mills, 1981, 1990), it has long been speculated that the production of their characteristic boulder deposits resulted from climate cycles, but their morphology has not been tied to a specific time or process until now. This work offers support for punctuated and climatically tuned deposition,

stability and resurfacing of boulders on boulder dominated hillslopes and channels in landscapes with moderate to high slope conditions in the southern Appalachians. It is thus an example of how climate oscillation inserts disequilibrium into the landscape cycle south of the glacial limits (e.g., Del Vecchio et al., 2018; Merritts & Rahnis, 2022; Spotila & Prince, 2022).

An appreciation of punctuated and climatically controlled boulder deposition and stability in the Appalachians can be applied to our developing understanding of changing hillslope stability resulting from contemporary global warming. As arctic and alpine bedrock landscapes with medium to high slope angles pass through periglacial frost cracking conditions during warming, we expect increased rockfall and talus deposition, as has been shown in many studies (Delunel et al., 2010; Haeberli et al., 2004; Hales & Roering, 2005; Krautblatter et al., 2012; Peizhen et al., 2001; Rowland et al., 2010; Sklar et al., 2017). What our work adds is the prediction that if continued warming causes these landscapes to exit the upper limits of the frost cracking window, and then, boulders deposited on the landscapes will stabilize and stagnate unless the climate substantially cools back to periglacial conditions. In this way, the impact of contemporary global warming can be expected to be a dominating influence on boulder armoured landscapes for a long time into the future.

6 | CONCLUSIONS

We determined cosmogenic exposure ages from large boulders on hillslopes and in channels in the Virginia Appalachians to resolve the timing of boulder deposition, residence time on hillslopes and in channels, and mechanisms driving their deposition and reworking. The correlation between measured boulder exposure ages (101.7 ± 6.9 ka to 10.8 ± 0.8 ka; $n = 23$) and the Wisconsin Glacial Stage and subsequent LIS deglaciation suggests a periglacial origin for deposition of large hillslope and channel boulders in the Virginia Appalachians. Frost cracking of bedrock and a decrease in the stabilization of ridge bedrock due to soil and vegetation changes under a periglacial climate are possible mechanisms driving the deposition of these large boulders.

The absence of exposure ages corresponding to the Last Interglacial Stage or the last 10 ka of the Holocene suggests that during interglacial and postglacial times there is no significant mechanism by which large boulders are deposited. The persistence of boulders with Wisconsin Glacial Stage exposure ages suggests that throughout the Holocene, boulders armouring hillslopes and channels have been largely immobile. The absence of exposure ages from the Illinoian or older Quaternary glacial stages suggest that hillslopes and channels are resurfaced with large boulders with each return to periglacial conditions as older boulders are moved off hillslopes via frost creep processes, broken down into smaller boulders, and/or are buried beneath younger periglacial boulders and postglacial soils. Boulders from the Blue Ridge province (16.9 ± 1.2 to 43.1 ± 3.0 ka; $n = 11$) have younger and more closely grouped exposure ages as compared to boulders from the Valley and Ridge province (10.8 ± 0.8 to 101.7 ± 6.9 ka; $n = 12$), which have a broader range of exposure ages that extend further back in the Wisconsin Stage. These differences may be a product of elevation and lapse rate-controlled temperature, slope angle control on frost creep processes, and/or percentage hillslope cover by large boulders.

The cyclic resurfacing of hillslopes and channels in the Virginia Appalachians with large boulders during periglacial times followed by their relative stability during interglacial times makes them an example of how periglacial climate oscillation is a significant driver of punctuated landscape disequilibrium. By investigating the lifecycle of periglacial boulder deposits in the southern Appalachians, we contribute to an appreciation of the climatically correlated timescales over which contemporary global warming is expected to be a dominating influence on boulder dominated alpine and arctic landscapes.

AUTHOR CONTRIBUTIONS

Michelle L. Fame: Conceptualization; funding acquisition; methodology; investigation; resources; writing—initial draft; writing—reviewing and editing. **Kristin D. Chilton**: Conceptualization; funding acquisition; investigation; resources; writing—reviewing and editing. **James A. Spotila**: Conceptualization; funding acquisition resources; writing—reviewing and editing. **Meredith A. Kelly**: Methodology; investigation; writing—reviewing and editing. **Summer A. Caton**: Funding acquisition; investigation; resources; writing—reviewing and editing.

ACKNOWLEDGEMENTS

Funding for this project was provided by a Purdue Rare Isotope Measurement Laboratory (PRIME) Seed Analysis grant awarded to K. Chilton and M. Fame and research funds associated with the Dartmouth Earth Sciences Obering Postdoctoral Fellowship. We appreciate assistance with field work from L. Basler, J. Baughman, and J. Cochran. Laboratory assistance from D. Davis and M. Stewart was funded by the Undergraduate Research Assistantships at Dartmouth (URAD) program. Discussion of ideas with J. Del Vecchio, M. Palucis, J. Marshall, and A. Dougherty as well as comments from two anonymous reviewers significantly shaped this work. We acknowledge the George Washington National Forest Service for allowing us to collect samples within the James Face Wilderness Area.

DATA AVAILABILITY STATEMENT

Data are available as a table within the paper, and any additional details can be obtained by contacting the corresponding author.

ORCID

Michelle L. Fame https://orcid.org/0000-0002-0305-6910

REFERENCES

Andersen, J.L., Egholm, D.L., Knudsen, M.F., Jansen, J.D. & Nielsen, S.B. (2015) The periglacial engine of mountain erosion–part 1: rates of frost cracking and frost creep. *Earth Surface Dynamics*, 3(4), 447–462. Available from: https://doi.org/10.5194/esurf-3-447-2015

Balco, G., Briner, J., Finkel, R.C., Rayburn, J.A., Ridge, J.C. & Schaefer, J.M. (2009) Regional beryllium-10 production rate calibration for late-glacial northeastern North America. *Quaternary Geochronology*, 4(2), 93–107. Available from: https://doi.org/10.1016/j.quageo.2008.09.001

Balco, G., Stone, J.O., Lifton, N.A. & Dunai, T.J. (2008) A complete and easily accessible means of calculating surface exposure ages or erosion rates from 10Be and 26Al measurements. *Quaternary Geochronology*, 3(3), 174–195. Available from: https://doi.org/10.1016/j.quageo.2007.12.001

Ballantyne, C. (2011) Periglacial and paraglacial processes and environments–edited by J Knight and S Harrison. *Area*, 43(2), 236–237. Available from: https://doi.org/10.1111/j.1475-4762.2010.00984_2.x

Bartholomew, M.J., Schultz, A.P., Lewis, S.E., McDowell, R.C. & Henika, W.S. (2000) *Digital geologic map of the Radford 30 × 60 minute quadrangle Virginia and West Virginia*. Charlottesville, Virginia: Commonwealth of Virginia Department of Mines, Mineral, and Energy, Division of Mineral Resources.

Bierman, P.R. (1994) Using in situ produced cosmogenic isotopes to estimate rates of landscape evolution: a review from the geomorphic perspective. *Journal of Geophysical Research - Solid Earth*, 1978–2012(99), 13885–13896.

Brown, C.E. & Spencer, E.W. (1981) Geologic map of the James River Face Wilderness, Bedford and Rockbridge counties Virginia (No. 1337-A).

Brown, E.T., Stallard, R.F., Larsen, M.C., Raisbeck, G.M. & Yiou, F. (1995) Denudation rates determined from the accumulation of in situ-produced 10 Be in the Luquillo Experimental Forest, Puerto Rico. *Earth and Planetary Science Letters*, 129(1-4), 193–202. Available from: https://doi.org/10.1016/0012-821X(94)00249-X

Carlson, A.E., Tarasov, L. & Pico, T. (2018) Rapid Laurentide ice-sheet advance towards southern last glacial maximum limit during marine isotope Stage 3. *Quaternary Science Reviews*, 196, 118–123. Available from: https://doi.org/10.1016/j.quascirev.2018.07.039

Chilton, K.D. & Spotila, J.A. (2020) Preservation of Valley and Ridge topography via delivery of resistant, ridge-sourced boulders to hillslopes and channels, Southern Appalachian Mountains, U.S.A. *Geomorphology*, 365, 107263. Available from: https://doi.org/10.1016/j.geomorph.2020.107263

Chmeleff, J., von Blanckenburg, F., Kossert, K. & Jakob, D. (2010) Determination of the 10Be half-life by multicollector ICP-MS and liquid scintillation counting. *Nuclear Instruments and Methods in Physics Research B*, 268(2), 192–199. Available from: https://doi.org/10.1016/j.nimb.2009.09.012

Clark, G.M. & Ciolkosz, E.J. (1988) Periglacial geomorphology of the Appalachian Highlands and Interior Highlands south of the glacial border—a review. *Geomorphology*, 1(3), 191–220. Available from: https://doi.org/10.1016/0169-555X(88)90014-1

Clark, P.U., Dyke, A.S., Shakun, J.D., Carlson, A.E., Clark, J., Wohlfarth, B., et al. (2009) The last glacial maximum. *Science* (1979, 325, 710–714.

Dalton, A.S., Margold, M., Stokes, C.R., Tarasov, L., Dyke, A.S., Adams, R.S., et al. (2020) An updated radiocarbon-based ice margin chronology for the last deglaciation of the North American Ice Sheet Complex. *Quaternary Science Reviews*, 234, 106223.

Dalton, A.S., Finkelstein, S.A., Forman, S.L., Barnett, P.J., Pico, T. & Mitrovica, J.X. (2019) Was the Laurentide Ice Sheet significantly reduced during marine isotope Stage 3? *Geology*, 47(2), 111–114. Available from: https://doi.org/10.1130/G45335.1

Dalton, A.S., Stokes, C.R. & Batchelor, C.L. (2022) Evolution of the Laurentide and Innuitian ice sheets prior to the Last Glacial Maximum (115 ka to 25 ka). *Earth-Science Reviews*, 224, 103875. Available from: https://doi.org/10.1016/j.earscirev.2021.103875

Del Vecchio, J., DiBiase, R.A., Denn, A.R., Bierman, P.R., Caffee, M.W. & Zimmerman, S.R. (2018) Record of coupled hillslope and channel response to Pleistocene erosion and deposition in a sandstone headwater valley, central Pennsylvania. *Bulletin of the Geological Society of America*, 130(11-12), 1903–1917. Available from: https://doi.org/10.1130/B31912.1

Delunel, R., van der Beek, P.A., Carcaillet, J., Bourlès, D.L. & Valla, P.G. (2010) Frost-cracking control on catchment denudation rates: insights from in situ produced 10Be concentrations in stream sediments (Ecrins-Pelvoux massif, French Western Alps). *Earth and Planetary Science Letters*, 293(1-2), 72–83. Available from: https://doi.org/10.1016/j.epsl.2010.02.020

Denn, A.R., Bierman, P.R., Zimmerman, S.R.H., Caffee, M.W., Corbett, L.B. & Kirby, E. (2018) Cosmogenic nuclides indicate that boulder fields are dynamic, ancient, multigenerational features. *GSA Today*, 28, 4–10. Available from: https://doi.org/10.1130/GSATG340A.1

DiBiase, R.A., Rossi, M.W. & Neely, A.B. (2018) Fracture density and grain size controls on the relief structure of bedrock landscapes. *Geology*, 46(5), 399–402. Available from: https://doi.org/10.1130/G40006.1

Doughty, A.M., Kaplan, M.R., Peltier, C. & Barker, S. (2021) A maximum in global glacier extent during MIS 4. *Quaternary Science Reviews*, 261, 106948. Available from: https://doi.org/10.1016/j.quascirev.2021.106948

Dunai, T.J. & Lifton, N.A. (2014) The nuts and bolts of cosmogenic nuclide production. *Elements*, 10(5), 347–350. Available from: https://doi.org/10.2113/gselements.10.5.347

Dyke, A.S. (2004) An outline of North American deglaciation with emphasis on central and northern Canada. *Developments in Quaternary Sciences*, 2, 373–424. Available from: https://doi.org/10.1016/S1571-0866(04)80209-4

Fichter, L.S., Whitmeyer, S.J., Bailey, C.M. & Burton, W. (2010). Stratigraphy, structure, and tectonics: an east-to-west transect of the Blue Ridge and Valley and Ridge provinces of northern Virginia and West Virginia. In: Fleeger, G.M. & Whitmeyer, S.J. (Eds.) *The mid-atlantic shore to the Appalachian highlands: Field trip guidebook for the 2010 Joint Meeting of the Northeastern and Southeastern GSA sections: Geological Society of America Field Guide 16* (pp. 103–125). Available from: https://doi.org/10.1130/2010.0016(05)

French, H.M. (2017) *The periglacial environment*, 4th edition, Chichester: John Wiley & Sons.

Girard, L., Gruber, S., Weber, S. & Beutel, J. (2013) Environmental controls of frost cracking revealed through in situ acoustic emission measurements in steep bedrock. *Geophysical Research Letters*, 40(9), 1748–1753. Available from: https://doi.org/10.1002/grl.50384

Glade, R.C. & Anderson, R.S. (2018) Quasi-steady evolution of hillslopes in layered landscapes: an analytic approach. *Journal of Geophysical Research - Earth Surface*, 123(1), 26–45. Available from: https://doi.org/10.1002/2017JF004466

Glade, R.C., Anderson, R.S. & Tucker, G.E. (2017) Block-controlled hillslope form and persistence of topography in rocky landscapes. *Geology*, 45(4), 311–314. Available from: https://doi.org/10.1130/G38665.1

Gosse, J.C. & Phillips, F.M. (2001) Terrestrial in situ cosmogenic nuclides: theory and application. *Quaternary Science Reviews*, 20(14), 1475–1560. Available from: https://doi.org/10.1016/S0277-3791(00)00171-2

Granger, D.E., Riebe, C.S., Kirchner, J.W. & Finkel, R.C. (2001) Modulation of erosion on steep granitic slopes by boulder armoring, as revealed by cosmogenic 26Al and 10Be. *Earth and Planetary Science Letters*, 186(2), 269–281. Available from: https://doi.org/10.1016/S0012-821X(01)00236-9

Haeberli, W., Huggel, C., Kääb, A., Zgraggen-Oswald, S., Polkvoj, A., Galushkin, I., et al. (2004) The Kolka-Karmadon rock/ice slide of 20 September 2002: an extraordinary event of historical dimensions in North Ossetia, Russian Caucasus. *Journal of Glaciology*, 50(171), 533–546. Available from: https://doi.org/10.3189/172756504781829710

Hale, P.A. & Shakoor, A. (2003) A laboratory investigation of the effects of cyclic heating and cooling, wetting and drying, and freezing and thawing on the compressive strength of selected sandstones. *Environmental and Engineering Geoscience*, 9(2), 117–130. Available from: https://doi.org/10.2113/9.2.117

Hales, T.C. & Roering, J.J. (2005) Climate-controlled variations in scree production, Southern Alps, New Zealand. *Geology*, 33(9), 701–704. Available from: https://doi.org/10.1130/G21528.1

Hancock, G.S., Anderson, R.S., Chadwick, O.A. & Finkel, R.C. (1999) Dating fluvial terraces with 10Be and 26Al profiles: application to the Wind River, Wyoming. *Geomorphology*, 27(1-2), 41–60. Available from: https://doi.org/10.1016/S0169-555X(98)00089-0

Horton, J.D., 2017. The state geologic map compilation (sgmc) geodatabase of the conterminous United States.

Krautblatter, M., Huggel, C., Deline, P. & Hasler, A. (2012) Research perspectives on unstable high-alpine bedrock permafrost: measurement, modelling and process understanding. *Permafrost and Periglacial Processes*, 23(1), 80–88. Available from: https://doi.org/10.1002/ppp.740

Lal, D. (1991) Cosmic ray labeling of erosion surfaces: in situ nuclide production rates and erosion models. *Earth and Planetary Science Letters*, 104(2-4), 424–439. Available from: https://doi.org/10.1016/0012-821X(91)90220-C

Lal, D., Pavich, M., Gu, Z.Y., Jull, A.J.T., Caffee, M., Finkel, R. & Southern, J., 1996. Recent erosional history of a soil profile based on cosmogenic

in-situ radionuclides 14C and 10Be. Earth processes: Reading the isotopic code 371–376.

Li, Y. (2018) Determining topographic shielding from digital elevation models for cosmogenic nuclide analysis: a GIS model for discrete sample sites. *Journal of Mountain Science*, 15(5), 939–947. Available from: https://doi.org/10.1007/s11629-018-4895-4

Lindgren, A., Hugelius, G., Kuhry, P., Christensen, T.R. & Vandenberghe, J. (2016) Gis-based maps and area estimates of northern hemisphere permafrost extent during the last glacial maximum. *Permafrost and Periglacial Processes*, 27(1), 6–16. Available from: https://doi.org/10.1002/ppp.1851

Lisiecki, L.E. & Raymo, M.E. (2005) A Pliocene-Pleistocene stack of 57 globally distributed benthic δ18O records. *Paleoceanography*, 20(1), n/a. Available from: https://doi.org/10.1029/2004PA001071

Lowe, J.J. & Walker, M.J.C. (2015) *Reconstructing quaternary environments*, 3rd edition, London: Routledge. Available from: https://doi.org/10.4324/9781315797496

Marsh, B. (1987) Pleistocene pingo scars in Pennsylvania. *Geology*, 15(10), 945–947. Available from: https://doi.org/10.1130/0091-7613(1987)15<945:PPSIP>2.0.CO;2

Marshall, J.A., Roering, J.J., Rempel, A.W., Shafer, S.L. & Bartlein, P.J. (2021) Extensive frost weathering across unglaciated North America during the Last Glacial Maximum. *Geophysical Research Letters*, 48(5), e2020GL090305. Available from: https://doi.org/10.1029/2020GL090305

Maxwell, J.A. & Davis, M.B. (1972) Pollen evidence of pleistocene and holocene vegetation on the Allegheny plateau, Maryland. *Quaternary Research*, 2(4), 506–530. Available from: https://doi.org/10.1016/0033-5894(72)90089-0

Merritts, D.J. & Rahnis, M.A. (2022) Pleistocene periglacial processes and landforms, mid-Atlantic region, eastern United States. *Annual Review of Earth and Planetary Sciences*, 50(1), 541–592. Available from: https://doi.org/10.1146/annurev-earth-032320-102849

Mills, H.H. (1981) Boulder deposits and the retreat of mountain slopes, or 'gully gravure' revisited. *Journal of Geology*, 89(5), 649–660. Available from: https://doi.org/10.1086/628628

Mills, H.H. (1989) Hollow form as a function of boulder size in the Valley and Ridge province, southwestern Virginia. *Geology*, 17(7), 595–598. Available from: https://doi.org/10.1130/0091-7613(1989)017<0595:HFAAFO>2.3.CO;2

Mills, H.H. (1990) Thickness and character of regolith on mountain slopes in the vicinity of Mountain Lake, Virginia, as indicated by seismic refraction, and implications for hillslope evolution. *Geomorphology*, 3(2), 143–157. Available from: https://doi.org/10.1016/0169-555X(90)90042-O

Mills, H.H. (2003) Inferring erosional resistance of bedrock units in the East Tennessee mountains from digital elevation data. *Geomorphology*, 55(1-4), 263–281. Available from: https://doi.org/10.1016/S0169-555X(03)00144-2

Murton, J.B., Peterson, R. & Ozouf, J.C. (2006) Bedrock fracture by ice segregation in cold regions. *Science*, 1979(314), 1127–1129. Available from: https://doi.org/10.1126/science.1132127

Nelson, K.J.P., Nelson, F.E. & Walegur, M.T. (2007) Periglacial Appalachia: palaeoclimatic significance of blockfield elevation gradients, eastern USA. *Permafrost and Periglacial Processes*, 18(1), 61–73. Available from: https://doi.org/10.1002/ppp.574

New, M., Lister, D., Hulme, M. & Makin, I. (2002) A high-resolution data set of surface climate over global land areas. *Climate Research*, 21, 1–25. Available from: https://doi.org/10.3354/cr021001

Nishiizumi, K., Imamura, M., Caffee, M.W., Southon, J.R., Finkel, R.C. & McAninch, J., 2007. Absolute calibration of 10Be AMS standards: nuclear instruments and methods in physical research section, v. 258, no. 2, 403–413.

Otvos, E.G. (2015) The last interglacial stage: definitions and marine highstand, North America and Eurasia. *Quaternary International*, 383, 158–173. Available from: https://doi.org/10.1016/j.quaint.2014.05.010

Peizhen, Z., Molnar, P. & Downs, W.R. (2001) Increased sedimentation rates and grain sizes 2-4 Myr ago due to the influence of climate change on erosion rates. *Nature*, 410(6831), 891–897. Available from: https://doi.org/10.1038/35073504

Portenga, E.W. & Bierman, P.R. (2011) Understanding Earth's eroding surface with 10 be. *GSA Today*, 21(8), 4–10. Available from: https://doi.org/10.1130/G111A.1

Portenga, E.W., Bierman, P.R., Rizzo, D.M. & Rood, D.H. (2013) Low rates of bedrock outcrop erosion in the Central Appalachian mountains inferred from in situ 10Be. *Bulletin of the Geological Society of America*, 125(1-2), 201–215. Available from: https://doi.org/10.1130/B30559.1

Potter, N., Jr. & Moss, J.H. (1968) Origin of the Blue Rocks block field and adjacent deposits, Berks County, Pennsylvania. *Geological Society of America Bulletin*, 79(2), 255–262. Available from: https://doi.org/10.1130/0016-7606(1968)79[255:OOTBRB]2.0.CO;2

Prince, P.S., Bartholomew, M.J. & Schultz, A.P. (2019) *Geologic Map of the Newport Quadrangle, Virginia*. Charlottesville, Virginia: Virginia Department of Mines, Minerals, and Energy.

Raymond, L.A., Webb, J.R.F. & Love, A.B., 2014. The Rose Hill formation and associated Tuscarora and Keefer sandstones of Clinch Mountain wildlife management area, southwestern Virginia, USA: issues of stratigraphic variation and diagenesis. Southeastern geology 50.

Rempel, A.W., Marshall, J.A. & Roering, J.J. (2016) Modeling relative frost weathering rates at geomorphic scales. *Earth and Planetary Science Letters*, 453, 87–95. Available from: https://doi.org/10.1016/j.epsl.2016.08.019

Ridge, J.C., Balco, G., Bayless, R.L., Beck, C.C., Carter, L.B., Dean, J.L., et al. (2012) The new North American varve chronology: a precise record of southeastern Laurentide Ice Sheet deglaciation and climate, 18.2-12.5 kyr BP, and correlations with Greenland ice core records. *American Journal of Science*, 312(7), 685–722. Available from: https://doi.org/10.2475/07.2012.01

Rowland, J.C., Jones, C.E., Altmann, G., Bryan, R., Crosby, B.T., Geernaert, G.L., et al. (2010) Arctic landscapes in transition: responses to thawing permafrost. *Eos* (Washington DC, 91(26), 229–230. Available from: https://doi.org/10.1029/2010EO260001

Sass, O. (2005) Rock moisture measurements: techniques, results, and implications for weathering. *Earth Surface Processes and Landforms*, 30(3), 359–374. Available from: https://doi.org/10.1002/esp.1214

Schultz, A.P., Stanley, C.B., Gaithright, T.M., II, Rader, E.K., Bartholmew, M.J., Lewis, S.E., et al. (1986) *Geologic Map of Giles County, Virginia*. Charlottesville, Virginia: Virginia Department of Mines, Minerals, and Energy Resources.

Schwab, F.L. (1970) Origin of the Antietam Formation (Late Precambrian?–Lower Cambrian), Central Virginia. *Journal of Sedimentary Research*, 40(1). Available from: https://doi.org/10.1306/74D71F46-2B21-11D7-8648000102C1865D

Shafer, S.L., Bartlein, P.J. & Izumi, K., 2021. PMIP3/CMIP5 lgm simulated temperature data for North America downscaled to a 10-km grid: US Geological Survey data release.

Shobe, C.M., Tucker, G.E. & Anderson, R.S. (2016) Hillslope-derived blocks retard river incision. *Geophysical Research Letters*, 43(10), 5070–5078. Available from: https://doi.org/10.1002/2016GL069262

Shobe, C.M., Tucker, G.E. & Rossi, M.W. (2018) Variable-threshold behavior in rivers arising from hillslope-derived blocks. *Journal of Geophysical Research - Earth Surface*, 123(8), 1931–1957. Available from: https://doi.org/10.1029/2017JF004575

Sklar, L.S. & Dietrich, W.E. (2001) Sediment and rock strength controls on river incision into bedrock. *Geology*, 29(12), 1087–1090. Available from: https://doi.org/10.1130/0091-7613(2001)029<1087:SARSCO>2.0.CO;2

Sklar, L.S., Riebe, C.S., Marshall, J.A., Genetti, J., Leclere, S., Lukens, C.L., et al. (2017) The problem of predicting the size distribution of sediment supplied by hillslopes to rivers. *Geomorphology*, 277, 31–49. Available from: https://doi.org/10.1016/j.geomorph.2016.05.005

Spotila, J.A. & Prince, P.S. (2022) Geomorphic complexity and the case for topographic rejuvenation of the Appalachian Mountains. *Geomorphology*, 417, 108449. Available from: https://doi.org/10.1016/j.geomorph.2022.108449

Staiger, J.W., Gosse, J., Little, E.C., Utting, D.J., Finkel, R., Johnson, J.V., et al. (2006) Glacial erosion and sediment dispersion from detrital cosmogenic nuclide analyses of till. *Quaternary Geochronology*, 1(1), 29–42. Available from: https://doi.org/10.1016/j.quageo.2006.06.009

Stone, J.O. (2000) Air pressure and cosmogenic isotope production. *Journal of Geophysical Research - Solid Earth* (1978–2012, 105, 23753–23759. Available from: https://doi.org/10.1029/2000JB900181

Thaler, E.A. & Covington, M.D. (2016) The influence of sandstone caprock material on bedrock channel steepness within a tectonically passive setting: Buffalo National River Basin, Arkansas, USA. *Journal of Geophysical Research - Earth Surface*, 121(9), 1635–1650. Available from: https://doi.org/10.1002/2015JF003771

Thompson, P., Schwarcz, H.P. & Ford, D.C. (1976) Stable isotope geochemistry, geothermometry, and geochronology of speleothems from West Virginia. *Geological Society of America Bulletin*, 87(12), 1730–1738. Available from: https://doi.org/10.1130/0016-7606(1976)87<1730:SIGGAG>2.0.CO;2

von Blanckenburg, F. & Willenbring, J.K. (2014) Cosmogenic nuclides: dates and rates of earth-surface change. *Elements*, 10(5), 341–346. Available from: https://doi.org/10.2113/gselements.10.5.341

Walder, J. & Hallet, B. (1985) Theoretical model of the fracture of rock during freezing. *Bulletin of the Geological Society of America*, 96(3), 336–346. Available from: https://doi.org/10.1130/0016-7606(1985)96<336:ATMOTF>2.0.CO;2

Walder, J.S. & Hallet, B. (1986) The physical basis of frost weathering: toward a more fundamental and unified perspective. *Arctic and Alpine Research*, 18(1), 27–32. Available from: https://doi.org/10.2307/1551211

Ward, D.J., Spotila, J.A., Hancock, G.S. & Galbraith, J.M. (2005) New constraints on the late Cenozoic incision history of the New River, Virginia. *Geomorphology*, 72(1-4), 54–72. Available from: https://doi.org/10.1016/j.geomorph.2005.05.002

Watts, W.A. (1979) Late Quaternary vegetation of central Appalachia and the New Jersey coastal plain. *Ecological Monographs*, 49(4), 427–469. Available from: https://doi.org/10.2307/1942471

Webb, T. (1987) The appearance and disappearance of major vegetational assemblages: long-term vegetational dynamics in eastern North America. *Vegetatio*, 69(1-3), 177–187. Available from: https://doi.org/10.1007/BF00038699

Whittecar, G.R. & Ryter, D.W. (1992) Boulder streams, debris fans, and Pleistocene climate change in the Blue Ridge Mountains of central Virginia. *Journal of Geology*, 100(4), 487–494. Available from: https://doi.org/10.1086/629600

Williams, J.W., Shuman, B.N., Webb, T., III, Bartlein, P.J. & Leduc, P.L. (2004) Late-Quaternary vegetation dynamics in North America: scaling from taxa to biomes. *Ecological Monographs*, 74(2), 309–334. Available from: https://doi.org/10.1890/02-4045

SUPPORTING INFORMATION

Additional supporting information can be found online in the Supporting Information section at the end of this article.

How to cite this article: Fame, M.L., Chilton, K.D., Spotila, J.A., Kelly, M.A. & Caton, S.A. (2023) Periglacial resurfacing of hillslopes and channels with large boulders in the Virginia Appalachians. *Earth Surface Processes and Landforms*, 1–19. Available from: https://doi.org/10.1002/esp.5713